EUROPEAN ORGANIZATION FOR NUCLEAR RESEARCH (CERN)

Measurement of the Drell–Yan Cross Section in pp Collisions at $\sqrt{s} = 7\,\text{TeV}$

The CMS Collaboration[*]

Abstract

The Drell–Yan differential cross section is measured in pp collisions at $\sqrt{s} = 7$ TeV, from a data sample collected with the CMS detector at the LHC, corresponding to an integrated luminosity of 36 pb^{-1}. The cross section measurement, normalized to the measured cross section in the Z region, is reported for both the dimuon and dielectron channels in the dilepton invariant mass range 15–600 GeV. The normalized cross section values are quoted both in the full phase space and within the detector acceptance. The effect of final state radiation is also identified. The results are found to agree with theoretical predictions.

[*]See Appendix A for the list of collaboration members

1 Introduction

The production of lepton pairs in hadron-hadron collisions via the Drell–Yan (DY) process is described in the standard model (SM) by the s-channel exchange of γ^*/Z. Theoretical calculations of the differential cross section $d\sigma/dM(\ell\ell)$, where $M(\ell\ell)$ is the dilepton invariant mass, are well established up to next-to-next-to-leading order (NNLO) [1–3]. Therefore, comparisons between calculations and precise experimental measurements provide stringent tests of perturbative quantum chromodynamics (QCD) and significant constraints on the evaluation of the parton distribution functions (PDFs). Furthermore, the production of DY lepton pairs constitutes a major source of background for $t\bar{t}$ and diboson measurements, as well as for searches for new physics, such as production of high mass dilepton resonances.

This paper presents a measurement of the differential DY cross section in proton-proton collisions at $\sqrt{s} = 7\,\text{TeV}$, based on dimuon and dielectron data samples collected in 2010 by the Compact Muon Solenoid (CMS) experiment at the Large Hadron Collider (LHC), corresponding to an integrated luminosity of $35.9 \pm 1.4\,\text{pb}^{-1}$. The results are given for the dilepton invariant mass range $15 < M(\ell\ell) < 600\,\text{GeV}$, corresponding to the Bjorken x range 0.0003–0.633 for the interacting partons, and complement the observations previously reported by the Tevatron collaborations [4–6]. To reduce systematic uncertainties, the results are normalized to the cross section in the Z region ($60 < M(\ell\ell) < 120\,\text{GeV}$) as determined in the same measurement. The inclusive Z cross section in the full phase space was measured previously by CMS [7].

In the analysis presented, the cross sections are calculated as

$$\sigma = \frac{N_\text{u}}{A\,\epsilon\,\rho\,\mathcal{L}},$$ (1)

where N_u is the unfolded background-subtracted yield, corrected for detector resolution. The values of the acceptance A and the efficiency ϵ are estimated from simulation, while ρ is a factor that accounts for differences in the detection efficiency between data and simulation. Knowledge of the integrated luminosity $\mathcal{L}$ is not required for the measurements described in this paper, since the cross sections are normalized to the Z region.

This paper is organized as follows: in Section 2 the CMS detector is described, with particular attention to the subdetectors used to identify charged leptons. Section 3 describes the data and Monte Carlo (MC) samples used in the analysis and the selection applied to identify the DY candidates. The signal extraction methods for the muon and electron channels, as well as the background contributions to the candidate samples are discussed in Section 4. Section 5 describes the analysis techniques used to unfold the detector resolution from the measurements. The calculation of the geometrical and kinematic acceptances together with the methods applied to determine the reconstruction, selection, and trigger efficiencies of the leptons within the experimental acceptance are presented in Section 6. Systematic uncertainties are discussed in Section 7. The calculation of the shapes of the DY invariant mass distributions are summarized in Section 8. In that section we report not only results in the full phase space but also results as measured within the fiducial and kinematic acceptance (both before and after final state QED radiation corrections), thereby eliminating the PDF uncertainties from the results.

2 The CMS Detector

A detailed description of the CMS detector and its performance can be found in Ref. [8]. The central feature of the CMS apparatus is a superconducting solenoid 13 m in length and

6 m in diameter, which provides an axial magnetic field of 3.8 T. Within the field volume are the silicon pixel and strip tracker, the crystal electromagnetic calorimeter (ECAL), and the brass/scintillator hadron calorimeter. Charged particle trajectories are measured by the tracker, covering the full azimuthal angle and pseudorapidity interval $|\eta| < 2.5$, where the pseudorapidity is defined as $\eta = -\ln\tan(\theta/2)$, with θ being the polar angle of the trajectory of the particle with respect to the counterclockwise beam direction. Muons are measured in the pseudorapidity range $|\eta| < 2.4$, with detection planes made using three technologies: drift tubes, cathode strip chambers, and resistive plate chambers. The muons associated with the tracks measured in the silicon tracker have a transverse momentum (p_T) resolution of about 2% in the muon p_T range relevant for the analysis presented in this paper. The ECAL consists of nearly 76 000 lead tungstate crystals, distributed in a barrel region ($|\eta| < 1.479$) and two endcap regions ($1.479 < |\eta| < 3$), and has an ultimate energy resolution better than 0.5% for unconverted photons with transverse energies (E_T) above 100 GeV. The electron energy resolution is better than 3% for the range of energies relevant for the measurement reported in this paper. A two-level trigger system selects the events for use in offline physics analysis.

3 Event Selection

The basic signature of the DY process is straightforward: two oppositely charged isolated leptons originating in the same primary vertex. The analysis presented in this paper is based on dilepton data samples selected by inclusive single-lepton triggers. The dimuon data sample was selected by a single-muon trigger with a p_T threshold ranging from 9 to 15 GeV, depending on the beam conditions. In the offline selection, one of the muons is required to match, in three-dimensional momentum space, a muon trigger candidate, and must have $|\eta| < 2.1$ and $p_T > 16$ GeV, to ensure that it is on the plateau of the trigger efficiency curve. The second muon is required to have $|\eta| < 2.4$ and $p_T > 7$ GeV. No muon isolation is required at the trigger level.

Muons are required to pass the standard CMS muon identification and quality criteria, based on the number of hits found in the tracker, the response of the muon chambers, and a set of matching criteria between the muon track parameters as determined by the inner tracker section of the detector and as measured in the muon chambers [9, 10]. These criteria ensure that only muons with well-measured parameters are selected for the analysis. To eliminate cosmic-ray muons, each muon is required to have an impact parameter in the transverse plane less than 2 mm with respect to the center of the interaction region, and the opening angle between the two muons must differ from π by more than 5 mrad. In order to reduce the fraction of muon pairs from (different) light-meson decays a common vertex for the two muons is fitted and the event is rejected if the dimuon vertex χ^2 probability is smaller than 2%. Finally, an isolation requirement is imposed on both muons, $I_{rel} = (\sum p_T(\text{tracks}) + \sum E_T(\text{had}))/p_T(\mu) < 0.15$, where $\sum p_T(\text{tracks})$ is the sum of the transverse momenta of all the additional tracker tracks and $\sum E_T(\text{had})$ is the sum of all transverse energies of hadronic deposits in a cone $\Delta R = \sqrt{(\Delta\phi)^2 + (\Delta\eta)^2} < 0.3$ centered on the muon direction and excluding the muon itself. Given that muons can radiate nearly collinear photons in a process referred to as final state electromagnetic radiation (FSR), deposits in the ECAL are not included in the definition. Otherwise an inefficiency would be introduced in the analysis.

For the electron analysis, events are selected with a trigger requiring at least one electron, with a minimum E_T ranging from 15 to 17 GeV, depending on the beam conditions. Electron reconstruction starts from clusters of energy deposited in the ECAL, and associates with them hits in the CMS tracker [11]. Energy-scale corrections are applied to individual electrons as described in Ref. [12]. The electron candidate is required to be consistent with a particle originating from

the primary vertex in the event. Electron identification criteria based on shower shape and track-cluster matching are applied to the reconstructed candidates. Electrons originating from photon conversions are rejected by eliminating those electrons for which a partner track consistent with a conversion hypothesis is found, and requiring no missing hits in the pixel detector, as discussed in Ref. [7]. Isolation requirements are imposed on each electron, according to $(\sum p_T(\text{tracks}) + \sum E_T(\text{had}) + \sum E_T(\text{em}))/p_T(\text{e}) < 0.1$, where $\sum p_T(\text{tracks})$ and $\sum E_T(\text{had})$ are defined as explained for muons, and $\sum E_T(\text{em})$ is the sum of the transverse energies of electromagnetic deposits in $\Delta R < 0.3$, excluding the electron candidate itself. The standard CMS isolation calculation for electrons also excludes ECAL energy deposits that are potentially created by FSR photons, while absorbing some of these deposits into electron objects. Thus, the FSR-related inefficiencies, present for muons, are avoided for electrons and ECAL information is used in the total isolation calculation. The criteria were optimized to maximize the rejection of misidentified electrons from QCD multijet production and nonisolated electrons from heavy-quark decays, while maintaining at least 80% efficiency for electrons from the DY process. More details are found in Ref. [7].

Electrons must be reconstructed in the ECAL barrel with $|\eta| < 1.44$ or in the ECAL endcaps with $1.57 < |\eta| < 2.5$. The leading electron is required to have $E_T > 20\,\text{GeV}$, while the second electron must have $E_T > 10\,\text{GeV}$. The leading electron in a candidate pair is required to match, in η and ϕ, a trigger electron candidate.

Event samples for simulation studies of electroweak processes involving W and Z production are produced with the NLO MC generator POWHEG [13–15] interfaced with the PYTHIA (v. 6.422) [16] parton-shower event generator, using the CT10 [17] parametrization of the PDFs. PYTHIA is also used for the FSR simulation. The QCD multijet background is generated with PYTHIA, and the $t\bar{t}$ background is simulated using MADGRAPH (v. 4.4.12) [18] and PYTHIA at leading order using the CTEQ 6L PDF set [19] for both samples. Generated events are processed through the full GEANT4 [20] detector simulation, trigger emulation, and event reconstruction chain.

The observed invariant mass distributions, in the dimuon and dielectron channels, are shown in Fig. 1. Thirteen mass bins are used to cover the observable dilepton mass spectrum. These are chosen not only to be wide enough to minimize the influence of the mass resolution but also to provide good statistical power. The mass resolution varies between a few hundred MeV at the low invariant masses covered and several tens of GeV at the high end of the spectrum. The mass bins have unequal widths.

4　Backgrounds

Several physical and instrumental backgrounds contribute to both the dimuon and dielectron analyses. The main backgrounds at high dilepton invariant masses are caused by $t\bar{t}$ and diboson production, while at invariant masses below the Z peak, DY production of $\tau^+\tau^-$ pairs becomes the dominant background. At low dimuon invariant masses, most background events are QCD multijet events. The expected shapes and relative yields of these several dilepton sources can be seen in Fig. 1.

For the dimuon channel, the electroweak and $t\bar{t}$ backgrounds are evaluated through simulation studies, expected to provide a good description of the real contributions. This is also verified by related studies in the electron channel presented below. In contrast, the QCD background is evaluated from data by two independent methods. The first estimates the yield of opposite-sign (OS) background muon pairs by scaling the yield of same-sign (SS) pairs. The scaling
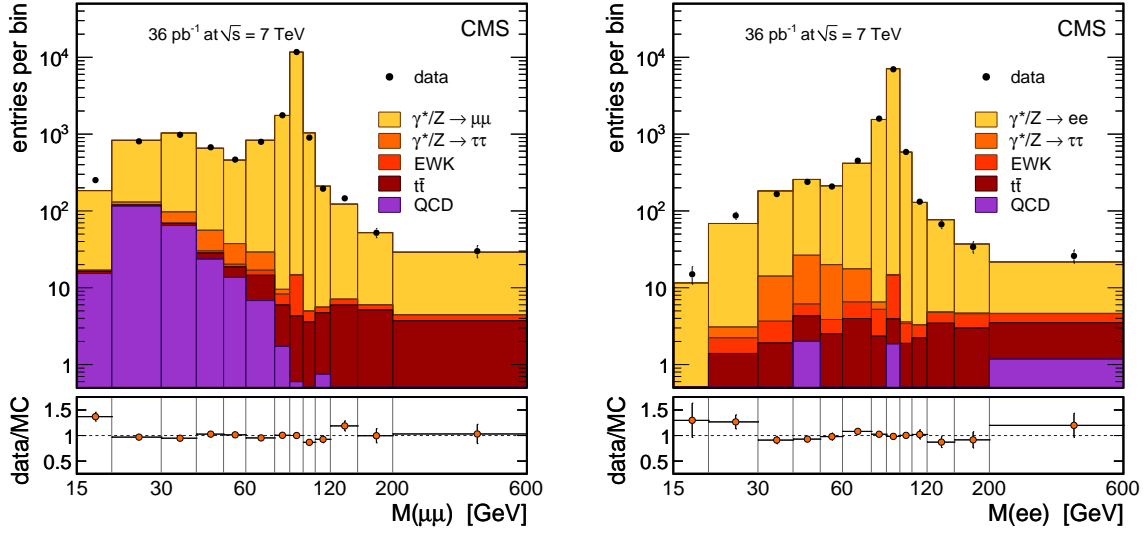
Figure 1: The observed dimuon (left) and dielectron (right) invariant mass spectra. No corrections are applied to the distributions. The points with error bars represent the data, while the various contributions from simulated events are shown as stacked histograms. By "EWK" we denote $Z/\gamma^* \to \tau\tau$, $W \to \ell\nu$, and diboson production. The "QCD" contribution results from processes associated with QCD and could be genuine or misidentified leptons. The lower panels show the ratios between the measured and the simulated distributions including the statistical uncertainties from both.

is based on information from the ratio of OS/SS events when one of the muons is not isolated (a sample dominated by background), and the MC prediction that the same ratio holds when both muons are isolated. Statistical uncertainties in all the cases are propagated to the final background estimate. The second method, which is more precise, is based on the signal/background discriminating variable I_{rel}. We obtain p_T-dependent isolation distributions (templates) from almost pure samples of background and signal events, respectively composed of SS and OS muon pairs. The latter consist of events in the Z mass peak surviving tight quality selection criteria. A superposition of these two shape distributions is fitted to the observed isolation distributions of the two muons, for each invariant mass bin. The dimuon invariant mass distribution of the QCD background is obtained as the weighted average of the estimates from the two methods.

There are two categories of dielectron backgrounds: the first category contributes candidates composed of two genuine electrons and the second contributes candidates in which at least one particle is a misidentified electron. Most of the genuine dielectron background is due to $t\bar{t}$, WW, and tW production, as well as DY production of $\tau^+\tau^-$ pairs. We estimate the contribution from these processes with a sample of $e^\pm\mu^\mp$ events having the same physical origin. This signal-free sample contains approximately twice the estimated number of background events contaminating the e^+e^- sample, and provides an evaluation of the background level that agrees with the estimate based on simulation studies. The genuine dielectron background from WZ and ZZ production is estimated from simulation. The misidentified electron backgrounds originate from QCD multijet and W+jet events. These sources of background are relatively small because of the tight electron identification and kinematic requirements, and are estimated from data based on the probability that jets or random energy deposits in the calorimeters emulate electron candidates [21].

The background estimates in the dimuon and dielectron channels are tabulated in Section 5 (Tables 1 and 2, respectively).

5 Detector Resolution Effects and Unfolding

The effects of the detector resolution on the observed dilepton spectra are corrected through an unfolding procedure. The original invariant mass spectrum is related to the observed one (in the limit of no background) by

$$N_{\mathrm{obs},i} = \sum_k T_{ik}\, N_{\mathrm{true},k},$$ (2)

where N_i is the event count in a given invariant mass bin i. The element T_{ik} of the "response matrix" T is the probability that an event with an original invariant mass in the bin k is reconstructed with an invariant mass in the bin i. The original invariant mass spectrum is obtained by inverting the response matrix and calculating [22, 23]

$$N_{\mathrm{u},k} \equiv N_{\mathrm{true},k} = \sum_i (T^{-1})_{ki}\, N_{\mathrm{obs},i}.$$ (3)

This procedure is sufficient in the analysis reported in this paper because the response matrix is nonsingular and nearly diagonal. Two extra dilepton invariant mass bins are included in the unfolding procedure, to account for events observed with $M(\ell\ell) < 15$ GeV or $M(\ell\ell) > 600$ GeV.

The response matrix is calculated using the simulated sample of DY events, defining the "true mass" as the "generator level" dilepton invariant mass, after FSR. Only the selected events in the sample are used to calculate the response matrix. The loss of events caused by reconstruction inefficiencies or limited acceptance is factored out from the unfolding procedure and taken into account by means of efficiency and acceptance factors in a subsequent step. Events generated with a dilepton invariant mass in the window of the analysis but reconstructed with an invariant mass too small (below 15 GeV) or too large (above 600 GeV) contribute to the response matrix. Events generated outside this window but reconstructed inside it are also accounted for. The sum of probabilities in the columns of the response matrix plus the probabilities of the bins with too small and too large invariant masses is constrained to be 100%.

The response matrices are nearly diagonal. The few significant off-diagonal elements present are found immediately next to the diagonal elements. Almost all off-diagonal elements are less than 0.1 for the muon channel and less than 0.3 for the electron channel, as shown in Fig. 2. The response matrices in both lepton channels are invertible.

The larger off-diagonal elements in the response matrix for the electron channel reflect a larger crossfeed among neighboring bins due to the following two factors. First, the detector resolution is worse for electrons than for muons. Second, the electron reconstruction algorithm attributes the four-momenta of some FSR photons to the electrons. Thus, for electrons, unfolding removes not only the effect of detector resolution on the invariant mass but also the effect of FSR photons in the electron reconstruction, yielding the original mass spectrum after FSR. The calculation of the original mass spectrum before FSR from the spectrum resulting from the unfolding procedure is done in a separate step through FSR corrections and is described in the next section.

The yields before and after background subtraction and the unfolding corrections are given in Tables 1 and 2.
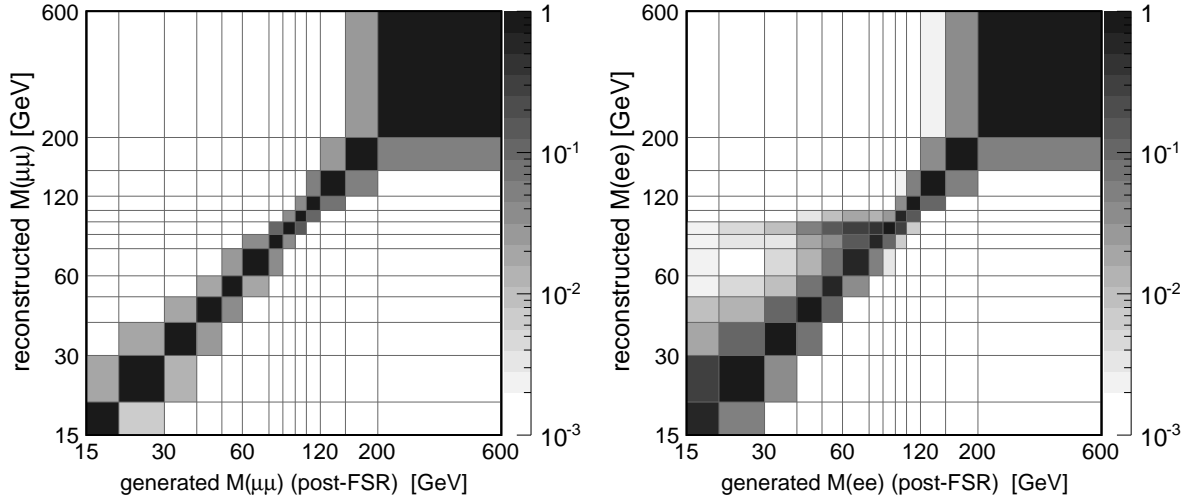
Figure 2: The response matrices for the muon (left) and electron (right) channels from simulation.

6 Acceptance and Efficiency

The reconstructed dilepton invariant mass distributions cannot be directly compared to the spectra provided by the theoretical models, not only because of the limited acceptance coverage of the detector but also because the observed spectra are affected by FSR, a process usually not included in the calculations. We define "pre-FSR" and "post-FSR" as labels to be attached to any quantity referred to before and after the FSR effects occur. The measurement of $d\sigma/dM(\ell\ell)$ therefore requires a two-step correction procedure. First, the measured, post-FSR spectra are corrected for acceptance, when applicable, and detector efficiencies. Then the (acceptance and) efficiency corrected spectra are themselves altered by a bin-by-bin FSR correction factor which relates the yields before and after the FSR takes place. These spectra can be compared to the calculations.

The geometrical and kinematic acceptance A is defined, using the simulated leptons after the FSR simulation, as $A \equiv N_{\text{acc}}/N_{\text{gen}}$, where N_{gen} is the number of generated events and N_{acc} is the corresponding number of events passing the standard p_{T} and η lepton requirements, in each dilepton invariant mass bin.

The efficiency ϵ is the fraction of events within the acceptance that pass the full selection, so that

$$A \cdot \epsilon \equiv \frac{N_{\text{acc}}}{N_{\text{gen}}} \cdot \frac{N_{\epsilon}}{N_{\text{acc}}} = \frac{N_{\epsilon}}{N_{\text{gen}}}, \tag{4}$$

where N_{ϵ} is the number of events surviving the reconstruction, selection, and identification requirements. The values of the product of acceptance and efficiency are obtained from simulation. A separate correction factor is determined from data and applied to the product, following the procedure used in the inclusive W and Z cross section measurements in CMS [7]. This factor, the efficiency correction, describes the difference between data and simulation in the efficiency to observe single leptons or dileptons.

The POWHEG simulation combines the next-to-leading-order (NLO) calculations with a parton showering which is insufficient to model fully the low invariant mass region of the dilepton spectra. The two high-p_{T} leptons required in the analysis must form a small angle at low mass

Table 1: Observed data yields, estimated backgrounds, and background-corrected and un-folded signal yields for DY production in the $\mu^+\mu^-$ channel. The QCD background is estimated from data whereas the "Other" background contributions (as indicated in Fig. 1) are based on simulation.

Invariant mass bin (GeV)	N_{obs}	Backgrounds		$N_{\text{obs}} - N_{\text{bg}}$	N_{u}
		QCD	Other		
15–20	253 ± 16	11 ± 8	1 ± 1	241 ± 18	243 ± 19
20–30	809 ± 28	59 ± 21	15 ± 4	735 ± 36	736 ± 37
30–40	986 ± 31	46 ± 15	30 ± 6	910 ± 36	907 ± 37
40–50	684 ± 26	22 ± 8	30 ± 6	632 ± 29	631 ± 30
50–60	471 ± 22	11 ± 7	25 ± 6	435 ± 24	436 ± 26
60–76	797 ± 28	7 ± 6	22 ± 5	768 ± 29	752 ± 31
76–86	1761 ± 42		6 ± 3	1755 ± 42	1471 ± 49
86–96	11786 ± 109		25 ± 6	11761 ± 109	12389 ± 119
96–106	909 ± 30		5 ± 3	904 ± 30	591 ± 38
106–120	194 ± 14		3 ± 2	191 ± 14	178 ± 17
120–150	145 ± 12		4 ± 3	141 ± 12	142 ± 13
150–200	53 ± 7		4 ± 3	49 ± 8	47 ± 9
200–600	30 ± 6		3 ± 2	27 ± 6	28 ± 6

and therefore the dilepton system gets significantly boosted, something to be compensated by hard gluon radiation in the transverse plane. This means that these low-mass events are of the type "γ^* + hard jet" at first order, and therefore the next order of correction (NNLO) becomes essential for a reliable estimate of acceptance corrections. To account for this, a correction is applied, determined from the ratio between the differential cross sections calculated at NNLO with FEWZ [24] and at NLO with POWHEG, both at pre-FSR level. These correction weights, obtained in bins of dilepton rapidity, p_T, and invariant mass, are applied on an event-by-event basis. The distributions obtained are used for all the simulation based estimations (acceptance, efficiency, FSR corrections) for DY, and this sample is referred to as "POWHEG matched to FEWZ (NNLO) distributions". This procedure changes the acceptance in the lowest invariant mass bin significantly (by about 50%), but has a small effect, not exceeding 3%, on the rest of the bins.

Figure 3 shows the variables A, ϵ, and $A \cdot \epsilon$ as functions of $M(\ell\ell)$ for dimuons (left) and dielectrons (right), the values being listed in Tables 3 and 4, respectively.

The FSR correction factors listed in Tables 3 and 4 for a given invariant mass range are obtained from simulation by dividing the post-FSR cross sections by the corresponding pre-FSR quantities. They are applied on (corrected) data as an additional step as described earlier in the section. The factors obtained within the detector acceptance and in the full phase space (as shown in the tables) are applied to the corresponding measurements. Systematic uncertainties related to the FSR simulation are discussed in Section 7.

The total dimuon event selection efficiency is factorized as

$$\varepsilon(\text{event}) = \varepsilon(\mu_1) \cdot \varepsilon(\mu_2) \cdot \varepsilon[\mu\mu|(\mu_1)\&(\mu_2)] \cdot \varepsilon(\text{event, trig}|\mu\mu), \qquad (5)$$

where $\varepsilon(\mu)$ is the single muon selection efficiency; $\varepsilon[\mu\mu|(\mu_1)\&(\mu_2)]$ is the dimuon selection efficiency, which includes the requirement that the two muon tracks be consistent with originating

Table 2: Observed data yields, estimated backgrounds, and background-corrected and unfolded signal yields for DY production in the e^+e^- channel.

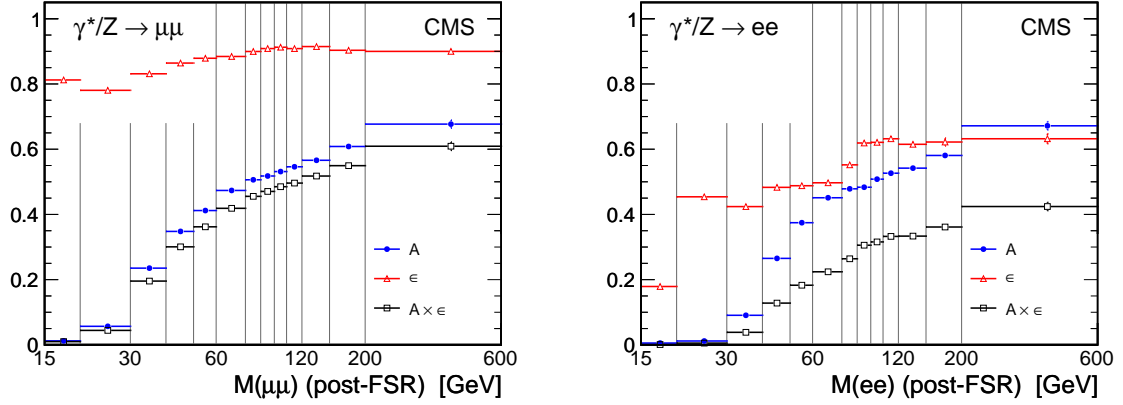| Invariant mass bin (GeV)	$N_{\rm obs}$	Backgrounds		$N_{\rm obs} - N_{\rm bg}$	$N_{\rm u}$
		genuine e^+e^-	misidentified e^+e^-		
15–20	16 $\pm$ 4	0.0 $\pm$ 0.2	0.4 $\pm$ 0.7	16 $\pm$ 4	16 $\pm$ 6
20–30	91 $\pm$ 10	2.5 $\pm$ 1.7	0.9 $\pm$ 1.1	88 $\pm$ 10	94 $\pm$ 12
30–40	179 $\pm$ 13	14.3 $\pm$ 4.6	1.5 $\pm$ 1.4	163 $\pm$ 14	164 $\pm$ 17
40–50	243 $\pm$ 16	31.4 $\pm$ 6.9	3.7 $\pm$ 2.7	208 $\pm$ 18	219 $\pm$ 22
50–60	211 $\pm$ 15	19.9 $\pm$ 5.2	3.9 $\pm$ 2.8	187 $\pm$ 16	234 $\pm$ 25
60–76	455 $\pm$ 21	22.4 $\pm$ 5.3	4.9 $\pm$ 3.3	428 $\pm$ 22	620 $\pm$ 45
76–86	1599 $\pm$ 40	8.5 $\pm$ 2.8	2.5 $\pm$ 2.1	1588 $\pm$ 40	1277 $\pm$ 89
86–96	6998 $\pm$ 84	12.5 $\pm$ 1.8	4.4 $\pm$ 3.1	6981 $\pm$ 84	7182 $\pm$ 117
96–106	587 $\pm$ 24	3.5 $\pm$ 1.8	2.1 $\pm$ 1.8	581 $\pm$ 24	441 $\pm$ 36
106–120	132 $\pm$ 11	3.2 $\pm$ 1.9	1.5 $\pm$ 1.4	127 $\pm$ 12	127 $\pm$ 15
120–150	67 $\pm$ 8	7.8 $\pm$ 3.1	2.0 $\pm$ 1.7	57 $\pm$ 9	53 $\pm$ 10
150–200	34 $\pm$ 6	5.5 $\pm$ 2.5	1.6 $\pm$ 1.4	27 $\pm$ 7	25 $\pm$ 7
200–600	26 $\pm$ 5	3.0 $\pm$ 1.9	1.4 $\pm$ 1.4	22 $\pm$ 6	21 $\pm$ 5

Figure 3: DY acceptance (blue, filled circles), efficiency (red, open triangles), and their product (black, open squares) per invariant mass bin, for the $\mu^+\mu^-$ (left) and e^+e^- (right) channels.

from a common vertex and that they satisfy the angular criteria; and $\varepsilon(\text{event}, \text{trig}|\mu\mu)$ is the efficiency of triggering an event including the efficiency that an identified muon is matched to a trigger object. The single muon efficiency is factorized as

$$\varepsilon(\mu) = \varepsilon(\text{track}|\text{accepted}) \cdot \varepsilon(\text{reco} + \text{id}|\text{track}) \cdot \varepsilon(\text{iso}|\text{reco} + \text{id}), \tag{6}$$

where $\varepsilon(\text{track}|\text{accepted})$ is the offline track reconstruction efficiency in the tracker detector; $\varepsilon(\text{reco} + \text{id}|\text{track})$ is the muon reconstruction and identification efficiency; and $\varepsilon(\text{iso}|\text{reco} + \text{id})$ is the muon isolation efficiency. The trigger efficiency $\varepsilon(\text{event}, \text{trig}|\mu\mu)$ is given by

$$\varepsilon(\text{event}, \text{trig}|\mu\mu) = \varepsilon(\mu_1, \text{trig}|\mu_1) + \varepsilon(\mu_2, \text{trig}|\mu_2) - \varepsilon(\mu_1, \text{trig}|\mu_1) \cdot \varepsilon(\mu_2, \text{trig}|\mu_2), \tag{7}$$

where $\varepsilon(\mu, \text{trig}|\mu)$ is the efficiency of an offline selected muon to fire the trigger.

Table 3: DY acceptance and acceptance times efficiency per invariant mass bin for the $\mu^+\mu^-$ channel. In addition, the FSR correction factors are given. All uncertainties are statistical.

Invariant mass bin (GeV)	Acceptance (%)	Acc × Eff (%)	FSR correction (%)	FSR correction in the acceptance (%)
15–20	1.23 ± 0.01	1.00 ± 0.01	97.28 ± 0.02	96.30 ± 0.02
20–30	5.69 ± 0.03	4.44 ± 0.03	97.28 ± 0.02	97.99 ± 0.02
30–40	23.5 ± 0.1	19.6 ± 0.1	98.43 ± 0.03	98.77 ± 0.03
40–50	34.8 ± 0.2	30.1 ± 0.2	104.0 ± 0.1	105.9 ± 0.1
50–60	41.2 ± 0.2	36.2 ± 0.2	120.2 ± 0.3	125.1 ± 0.3
60–76	47.4 ± 0.2	41.9 ± 0.2	166.4 ± 0.5	175.1 ± 0.6
76–86	50.6 ± 0.1	45.5 ± 0.1	167.1 ± 0.4	169.8 ± 0.4
86–96	51.8 ± 0.1	47.1 ± 0.1	91.63 ± 0.03	91.62 ± 0.03
96–106	53.1 ± 0.2	48.5 ± 0.2	88.0 ± 0.1	88.1 ± 0.1
106–120	54.6 ± 0.4	49.6 ± 0.4	91.3 ± 0.2	91.2 ± 0.2
120–150	56.6 ± 0.6	51.8 ± 0.6	93.2 ± 0.3	93.1 ± 0.3
150–200	60.8 ± 0.9	55.0 ± 0.9	94.3 ± 0.4	95.0 ± 0.4
200–600	67.7 ± 1.2	60.9 ± 1.3	92.8 ± 0.7	93.1 ± 0.6

Table 4: DY acceptance and acceptance times efficiency per invariant mass bin for the e^+e^- channel. In addition, the FSR correction factors are given. All uncertainties are statistical.

Invariant mass bin (GeV)	Acceptance (%)	Acc × Eff (%)	FSR correction (%)	FSR correction in the acceptance (%)
15–20	0.56 ± 0.01	0.10 ± 0.01	93.8 ± 0.1	98.7 ± 1.9
20–30	1.19 ± 0.01	0.54 ± 0.01	93.9 ± 0.2	102.9 ± 1.8
30–40	9.1 ± 0.1	3.6 ± 0.1	96.8 ± 0.3	109.5 ± 1.3
40–50	26.5 ± 0.2	12.8 ± 0.2	107.7 ± 0.6	117.8 ± 1.2
50–60	37.5 ± 0.2	18.3 ± 0.2	139.3 ± 1.0	156.2 ± 1.8
60–76	45.1 ± 0.2	22.4 ± 0.2	230.7 ± 1.4	256.3 ± 2.4
76–86	47.9 ± 0.1	26.4 ± 0.1	224.1 ± 1.0	235.0 ± 1.5
86–96	49.3 ± 0.1	30.6 ± 0.1	83.9 ± 0.1	85.6 ± 0.2
96–106	50.8 ± 0.2	31.6 ± 0.2	78.5 ± 0.5	80.1 ± 0.7
106–120	52.6 ± 0.4	33.3 ± 0.4	83.9 ± 1.0	85.2 ± 1.4
120–150	54.2 ± 0.6	33.4 ± 0.6	87.9 ± 1.4	88.5 ± 1.9
150–200	58.1 ± 0.9	36.1 ± 0.9	89.1 ± 2.2	90.3 ± 3.0
200–600	67.2 ± 1.3	42.4 ± 1.3	87.5 ± 3.2	88.9 ± 4.0

The track reconstruction efficiency is very high (99.5%). The angular criterion is nearly 100% efficient for signal DY events, and the vertex probability requirement is more than 98% efficient and has a negligible ($< 0.3\%$) dependence on $M(\ell\ell)$.

The muon reconstruction and identification efficiency is estimated using clean samples of muon pairs in the Z peak (tag and probe, T&P, method [7]). The properties of one muon are probed, after imposing tight requirements on the other one. To determine the isolation efficiency, the Lepton Kinematic Template Cones (LKTC) method [9] is applied. The essence of the LKTC method is to choose predefined directions in events with an underlying event environment similar to that of the signal sample. The isolation variable is defined as if these directions represent signal leptons, and the chosen isolation-based criteria are subsequently studied.

To describe the observed efficiency variations between data and simulation, efficiency correction factors are obtained in bins of p_T and η as the ratio of the efficiencies measured with data and with the simulated events:

$$\rho_{\mathrm{eff}}(p_T, \eta) = \frac{\varepsilon_{\mathrm{data}}(p_T, \eta)}{\varepsilon_{\mathrm{sim}}(p_T, \eta)}. \tag{8}$$

The corrections to the efficiencies in simulation are implemented by reweighting simulated events, with weights computed as $W = \rho_1^{\mathrm{reco}}\rho_2^{\mathrm{reco}}\rho_1^{\mathrm{iso}}\rho_2^{\mathrm{iso}}\rho^{\mathrm{trig}}$ where $\rho^{\mathrm{trig}} = (\epsilon_{\mathrm{data},1}^{\mathrm{trig}} + \epsilon_{\mathrm{data},2}^{\mathrm{trig}} - \epsilon_{\mathrm{data},1}^{\mathrm{trig}}\epsilon_{\mathrm{data},2}^{\mathrm{trig}})/(\epsilon_{\mathrm{MC},1}^{\mathrm{trig}} + \epsilon_{\mathrm{MC},2}^{\mathrm{trig}} - \epsilon_{\mathrm{MC},1}^{\mathrm{trig}}\epsilon_{\mathrm{MC},2}^{\mathrm{trig}})$. If $p_T < 16$ GeV or $|\eta| > 2.1$ for a given muon $i = 1, 2$, its trigger efficiency is set to zero.

The systematic uncertainty related to the efficiency correction is evaluated by generating one hundred variations of the (p_T, η) correction maps, where the weight in each (p_T, η) bin is obtained by adding to the original value a Gaussian-distributed shift of mean zero and width equal to the statistical uncertainty of the original correction factor (Eq. (8)). Signal corrected yields are evaluated using event weights obtained from each of the alternative correction maps and the RMS spread of the resulting values is taken as the systematic uncertainty. The systematic error computed with this procedure includes an irreducible statistical component, yielding a conservative uncertainty which also covers generous variations in the efficiency-correction shape. The resulting uncertainties are shown in Table 5.

The total event efficiency in the dielectron channel analysis is defined as the product of the two single electron efficiencies, which incorporate three factors: 1) the efficiency $\varepsilon_{\mathrm{reco}}$ to reconstruct an electron candidate from an energy deposit in the ECAL; 2) the efficiency $\varepsilon_{\mathrm{id}}$ for that candidate to pass the selection criteria, including identification, isolation, and conversion rejection; 3) the efficiency $\varepsilon_{\mathrm{trig}}$ for the leading electron to pass the trigger requirements. Each of these efficiencies is obtained from simulation and corrected by $\rho_{\mathrm{eff}}(p_T, \eta)$, as for the muon channel (Eq. (8)). The T&P method is used for all efficiency components. The event efficiency correction and its uncertainty are derived as for the muon channel by reweighting simulated events. The correction factors are listed in Table 5.

7   Systematic Uncertainties

Systematic uncertainties have been evaluated for each step in the determination of the dilepton invariant mass spectrum. The acceptance-related uncertainties are a special case as they only apply to the acceptance corrected results, i.e., results in the full phase space, and are approximately the same for the dimuon and dielectron channels (the FSR uncertainties are treated separately). The acceptance uncertainty resulting from the knowledge of the PDFs is estimated using PYTHIA with the CTEQ6.1 PDF set by a reweighting technique [25], with a negligible statistical uncertainty given the very large simulated sample. Since we are making a shape measurement, normalizing the DY cross section to the dilepton cross section in the Z region, the analysis only depends on the uncertainty of the *ratio* of acceptances, A_i / A_{norm}, where A_i is the acceptance for the invariant mass bin i and A_{norm} is the acceptance for the invariant mass region of the Z.

The uncertainty of the acceptance is estimated, for each dilepton invariant mass bin, using FEWZ, at NLO and NNLO accuracy in perturbative QCD. Variations of the factorization and renormalization scales lead to a systematic uncertainty smaller than 1% (at NNLO) for most of the invariant mass range used in the analysis presented here.

Table 5: Combined efficiency corrections for the muon and electron channels per mass bin. They account for the data vs. simulation differences in reconstruction, identification, isolation and trigger efficiencies.

Invariant mass	Combined efficiency correction	
bin (GeV)	Muon channel	Electron channel
15–20	0.917 ± 0.010	1.098 ± 0.087
20–30	0.915 ± 0.010	1.089 ± 0.091
30–40	0.918 ± 0.011	1.107 ± 0.103
40–50	0.931 ± 0.011	1.076 ± 0.081
50–60	0.943 ± 0.008	1.034 ± 0.053
60–76	0.952 ± 0.006	1.008 ± 0.033
76–86	0.958 ± 0.004	0.995 ± 0.024
86–96	0.960 ± 0.003	0.979 ± 0.019
96–106	0.961 ± 0.003	0.973 ± 0.018
106–120	0.961 ± 0.003	0.960 ± 0.018
120–150	0.956 ± 0.010	0.953 ± 0.019
150–200	0.957 ± 0.021	0.945 ± 0.020
200–600	0.957 ± 0.021	0.940 ± 0.020

Special care is needed to calculate the acceptance of low invariant mass dileptons, where differences between NLO and NNLO values can be significant, given the relatively high thresholds imposed on the transverse momentum of the leptons. Since the POWHEG MC (NLO) simulation, modified to match the FEWZ (NNLO) calculations, is used to calculate the acceptance corrections used in the analysis, an additional (model-dependent) systematic uncertainty on the acceptance calculation is determined from the observed differences in acceptances based on FEWZ spectra and POWHEG distributions matched to FEWZ. These differences are caused by variations in the kinematic distributions within the bins where bin sizes are chosen to take into account the limited reliability of perturbative QCD calculations in parts of the phase space. This systematic uncertainty reaches up to 10% in the dilepton invariant mass range considered in the analysis and is included in the comparison between the measurements and the theoretical expectations.

The dominant systematic uncertainty on the cross section measurement in the dimuon channel is the uncertainty on the background estimation, which is, however, relatively small given the low background levels. This uncertainty is evaluated from data using two independent background subtraction methods, as described in Section 4. The next most important uncertainties are related to the muon efficiency and to the muon momentum scale and resolution. The former is determined using the large sample of Z events decaying to dimuons. Uncertainties in the latter are mostly caused by residual misalignment between the muon chambers and the silicon tracker, potentially not reproduced in the simulation. The Z line shape is used to constrain the level of such possible limitations in the simulation. The momentum resolution and the momentum scale uncertainties are included in the unfolding procedure and, hence, the resulting shape is affected by these systematic effects. The level of the momentum scale uncertainty is evaluated by introducing a bias in the MC reconstruction and unfolding the resulting dimuon mass distribution with the unfolding matrix determined from the nominal (unbiased) MC sample. The bias is on the reconstructed invariant mass and is based on the maximal difference between MC and data Z peak positions as obtained with variations in the p_T and η requirements.

Studies of photons reconstructed near a muon in a DY event indicate that the FSR simulation

is remarkably accurate. A corresponding systematic uncertainty is evaluated by examining how the results change when the fraction of FSR events as well as the energy and angular distributions of the radiated photon are modified within proper statistical variations.

Other systematic effects that could affect the dimuon yield have been considered, such as the impact of additional soft pp collisions that occur in the same bunch crossing as the studied interaction and the effects of the dimuon vertex probability requirement and of residual data-simulation discrepancies. A combined uncertainty is reported for these "other" sources in Table 6, where all systematic uncertainties in the dimuon channel are listed.

Table 6: Summary of systematic uncertainties in the muon channel (in percent). The "Total" is a quadratic sum of all sources without "Acceptance". With the exception of "Acceptance", the numbers correspond to the individual measurements per bin and not the ratio to the Z region.

Invariant mass bin (GeV)	Efficiency correction	Background	Unfolding	FSR	Other	Total	Acceptance
15–20	1.1	3.6	0.4	1.5	1.0	4.2	+2.2/−3.0
20–30	1.1	3.1	0.2	1.1	1.0	3.6	+1.9/−3.2
30–40	1.2	1.9	0.1	0.7	1.0	2.6	+1.7/−3.0
40–50	1.2	1.7	0.2	0.7	1.0	2.4	+1.7/−2.9
50–60	0.8	2.1	0.2	0.5	0.5	2.4	+1.7/−2.8
60–76	0.6	1.0	0.2	1.4	0.5	1.9	+1.6/−2.6
76–86	0.4	0.2	1.7	2.0	0.5	2.7	+1.5/−2.5
86–96	0.3	0.05	0.2	0.5	0.5	0.8	+1.5/−2.4
96–106	0.3	0.4	3.8	0.5	0.5	3.9	+1.5/−2.4
106–120	0.3	1.4	0.7	0.5	3.0	3.4	+1.5/−2.3
120–150	1.1	2	0.4	0.5	1.0	2.6	+1.5/−2.1
150–200	2.1	6	0.9	0.5	1.0	6.5	+1.4/−1.8
200–600	2.1	10	0.1	0.5	1.0	10.3	+1.2/−1.4

In the electron channel, the leading systematic uncertainty is associated with the energy scale corrections of individual electrons. The corrections affect both the placement of a given candidate in a particular invariant mass bin and the likelihood of surviving the kinematic selection. The energy scale correction itself is calibrated to 2% precision for the dataset used. The associated error on signal event yields is calculated by varying the energy scale correction value within this amount and remeasuring the yields. This uncertainty takes its largest values for the bins just below and above the central Z peak bin because of bin migration. The energy scale uncertainty for the electron channel is on the order of 20 times larger than the momentum scale uncertainty for muons, for which the associated systematic uncertainties on the cross section are rather small.

The second leading uncertainty for electrons is caused by the uncertainty on the efficiency scale factors. The precision of the scale factor calibration is limited by the size of the data sample available for the T&P procedure. The systematic uncertainty on the scale factors as well as the resulting error on the normalized cross section are found with the same procedure as for the muon channel.

The dielectron background uncertainties are evaluated by comparing the background yields calculated as described in Section 4 with predictions from simulation. These uncertainties are only dominant at the highest invariant masses considered. The uncertainty associated with the unfolding procedure in the electron channel comes primarily from the uncertainty on the

Table 7: Summary of systematic uncertainties in the electron channel (in percent). The "Total" is a quadratic sum of all sources without "Acceptance". With the exception of "Acceptance", the numbers correspond to the individual measurements per bin and not the ratio to the Z region.

Invariant mass bin (GeV)	Energy scale	Efficiency correction	Background	Unfolding	Total	Acceptance
15–20	23.4	9.2	6.2	8.7	27.3	+2.1/−2.9
20–30	3.6	8.5	2.8	2.1	9.9	+1.7/−2.8
30–40	2.7	9.4	4.0	1.5	10.6	+1.5/−2.7
40–50	3.3	7.5	5.2	1.4	9.9	+1.5/−2.5
50–60	3.3	5.2	4.6	1.9	7.9	+1.5/−2.4
60–76	10.3	3.3	2.2	2.0	11.2	+1.4/−2.3
76–86	39.5	2.5	0.8	3.1	39.7	+1.3/−2.2
86–96	3.9	1.9	0.2	0.6	4.4	+1.2/−2.1
96–106	45.6	2.0	0.9	3.6	45.8	+1.3/−2.0
106–120	13.2	2.1	2.6	2.4	13.9	+1.3/−1.9
120–150	6.0	2.4	8.2	2.6	10.8	+1.3/−1.8
150–200	5.7	2.8	12.9	2.4	14.5	+1.2/−1.5
200–600	4.6	3.2	11.8	1.6	13.1	+1.0/−1.1

unfolding matrix elements due to imperfect simulation of detector resolution. This simulation uncertainty for electrons is significantly larger than for muons, leading to a larger systematic uncertainty on the normalized cross section. The uncertainties due to FSR effects are estimated with a method similar to that for the muon channel discussed above with similar values. Because of significantly higher systematic uncertainty for all mass bins for the electron channel than for the muon channel, the FSR related contribution to the electron channel systematic uncertainty is neglected.

The systematic uncertainties for the electron channel are summarized in Table 7. At present the dominant systematic uncertainties are driven by the limited size of calibration samples available for energy scale and efficiency scale factor calculations, and therefore the uncertainties could be reduced significantly with larger data samples.

8 Results

The DY cross section per invariant mass bin i, σ_i, is calculated according to Eq. (1).

In order to provide a measurement independent of the luminosity uncertainty and to reduce many systematic uncertainties, the σ_i is normalized to the cross section in the Z region, $\sigma_{\ell\ell}$, defined as the DY cross section in the invariant mass region $60 < M(\ell\ell) < 120$ GeV. The result of the analysis is presented as the ratio

$$R^i_{\text{post-FSR}} = \frac{N_{\text{u},i}}{A_i \, \varepsilon_i \, \rho_i} \Big/ \frac{N_{u,\text{norm}}}{A_{\text{norm}} \, \varepsilon_{\text{norm}} \, \rho_{\text{norm}}}, \tag{9}$$

where $N_{\text{u},i}$ is the number of events after the unfolding procedure, and the acceptances A_i, the efficiencies ϵ_i, and the corrections estimated from data, ρ_i, were defined earlier; $N_{u,\text{norm}}$, A_{norm}, $\varepsilon_{\text{norm}}$, and ρ_{norm} refer to the Z region. For both lepton channels, the cross sections in the Z region measured in this analysis are in excellent agreement with the previous CMS measurement [7].

In order to allow a more direct and precise comparison with theory predictions, the shape measured before the acceptance correction is also reported, thus eliminating PDF and theory uncertainties from the experimental results:

$$R^i_{\text{det, post-FSR}} = \frac{N_{\text{u},i}}{\varepsilon_i \, \rho_i} \Big/ \frac{N_{u,\text{norm}}}{\varepsilon_{\text{norm}} \, \rho_{\text{norm}}}. \tag{10}$$

The post-FSR shapes, $R_{\text{post-FSR}}$ and $R_{\text{det,post-FSR}}$, are modified by the FSR correction factors from Tables 3 and 4 to obtain the pre-FSR shapes, R and R_{det}, respectively. The shapes integrated in the normalization region are equal to one by construction.

The results are presented in Tables 8 and 9, respectively, for the dimuon and dielectron channels. The two shape measurements, shown in the last column of the tables, are in good agreement for 11 out of 13 invariant mass bins and remain statistically consistent (although marginally) for the remaining two bins, 40–50 GeV and 120–150 GeV.

As a semi-independent check, a measurement was performed using a data sample collected with a double-muon trigger with a lower p_{T} requirement of 7 GeV on each muon. The signal yield is increased tenfold at the lowest invariant masses at the expense of larger systematic uncertainties on the background. The result agrees with the measurement made with the single muon trigger, having a similar precision in the two lowest invariant mass bins.

Table 8: Results for the DY spectrum normalized to the Z region in the dimuon channel. The statistical and systematic uncertainties are summed in quadrature. $R_{\text{post-FSR}}$ and $R_{\text{det,post-FSR}}$ are calculated using Eqs. (9) and (10), respectively. The R_{det} and R are calculated using the FSR corrections given in Table 3.

Invariant mass bin (GeV)	$R_{\text{det,post-FSR}}$ (10^{-3})	R_{det} (10^{-3})	$R_{\text{post-FSR}}$ (10^{-3})	R (10^{-3})
15–20	18 ± 2	19 ± 2	772 ± 67	780 ± 69
20–30	58 ± 3	58 ± 3	528 ± 33	533 ± 34
30–40	67 ± 3	67 ± 3	147 ± 8	147 ± 8
40–50	44 ± 2	41 ± 2	66 ± 4	62 ± 4
50–60	30 ± 2	23 ± 2	37 ± 3	30 ± 2
60–76	51 ± 2	28 ± 1	55 ± 3	32 ± 2
76–86	97 ± 4	56 ± 3	98 ± 5	58 ± 3
86–96	803 ± 14	861 ± 15	799 ± 23	857 ± 26
96–106	38 ± 3	43 ± 3	37 ± 3	41 ± 3
106–120	12 ± 1	12 ± 1	11 ± 1	12 ± 1
120–150	9.2 ± 0.9	9.7 ± 1.0	8.4 ± 0.8	8.8 ± 0.9
150–200	3.1 ± 0.6	3.2 ± 0.7	2.6 ± 0.5	2.7 ± 0.6
200–600	1.8 ± 0.4	1.9 ± 0.5	1.4 ± 0.3	1.5 ± 0.4

The theoretical cross section is calculated with FEWZ and three sets of PDFs: CT10, CTEQ66 [26], and MSTW2008 [27]. The calculations include leptonic decays of Z bosons with full spin correlations as well as nonzero width effects and γ^*-Z interference. However, they do not simulate FSR effects. The calculations are cross-checked with the program DYNNLO, based on [2, 3], which offers features similar to FEWZ. The predictions for the shape of the DY spectrum agree well between the two programs, typically within 1%.

The uncertainties on the theoretical predictions due to the imprecise knowledge of the PDFs are calculated with the LHAGLUE interface to the PDF library LHAPDF [28, 29], using a reweighting technique with asymmetric uncertainties [25]. Since this is a shape measurement, and the

Table 9: Results for the DY spectrum normalized to the Z region in the dielectron channel. The statistical and systematic uncertainties are summed in quadrature. $R_{\text{post-FSR}}$ and $R_{\text{det,post-FSR}}$ are calculated using Eqs. (9) and (10), respectively. The R_{det} and R are calculated using the FSR corrections given in Table 4.

Invariant mass bin (GeV)	$R_{\text{det,post-FSR}}\ (10^{-3})$	$R_{\text{det}}\ (10^{-3})$	$R_{\text{post-FSR}}\ (10^{-3})$	$R\ (10^{-3})$
15–20	6 ± 3	6 ± 3	487 ± 230	508 ± 238
20–30	13 ± 2	13 ± 2	536 ± 96	559 ± 97
30–40	24 ± 4	22 ± 4	129 ± 22	131 ± 21
40–50	28 ± 4	24 ± 4	52 ± 8	47 ± 7
50–60	30 ± 5	19 ± 3	39 ± 6	27 ± 4
60–76	78 ± 12	30 ± 4	84 ± 13	36 ± 5
76–86	144 ± 60	61 ± 25	147 ± 60	64 ± 26
86–96	722 ± 62	839 ± 60	715 ± 62	834 ± 60
96–106	44 ± 21	55 ± 26	43 ± 20	53 ± 25
106–120	13 ± 3	15 ± 3	12 ± 2	14 ± 3
120–150	5.4 ± 1.2	6.0 ± 1.3	4.8 ± 1.1	5.4 ± 1.2
150–200	2.5 ± 0.8	2.8 ± 0.8	2.1 ± 0.6	2.3 ± 0.7
200–600	2.1 ± 0.6	2.4 ± 0.7	1.5 ± 0.5	1.7 ± 0.5

normalization of the spectrum is defined by the number of events in the Z region, the uncertainty is calculated for the yield ratio, Y_i/Y_{norm}, where Y_i is the predicted yield in the invariant mass bin i and Y_{norm} is the yield in the Z region. The uncertainties for these ratios are much smaller than those for the individual yields because of the correlations between Y_i and Y_{norm}, especially in the dilepton invariant mass region close to the Z mass.

The factorization and renormalization scales were varied between 0.5 and 2 times the dilepton invariant mass. The resulting variations of the cross sections at NNLO are much smaller than at NLO, and are less than 1.4% around the Z peak. The dependence of the DY cross section on the strong coupling constant α_s was evaluated by varying α_s between 0.116 and 0.120, using FEWZ and the CT10 PDF set. The cross section variations are at the percent level. Higher-order electroweak corrections for DY, evaluated with HORACE [30], showed a negligible influence (typically well below 1%) on the shape measurements in the investigated invariant mass range. The theoretical predictions from FEWZ at NNLO are presented in Table 10.

The results are also normalized to the invariant mass bin widths, ΔM_i, defining

$$r_i = \frac{R_i}{\Delta M_i}. \tag{11}$$

Assuming lepton universality, the dimuon and dielectron results for r_i are combined in a weighted average, using as weights the inverse of the respective squared total uncertainties, where the statistical and systematic uncertainties are added in quadrature.

The only expected source of correlation between the dimuon and dielectron results is due to the use of the same MC model for the acceptance and FSR corrections. Given that the uncertainties on these corrections are much smaller than most other uncertainties, especially in the dielectron channel, this correlation has a negligible influence on the combined results.

There are correlations between the invariant mass bins, induced by the various corrections applied in the analysis, especially those related to the efficiencies and resolutions. The efficiency corrections are highly correlated between adjacent invariant mass bins, since they tend

Table 10: Theoretical predictions at NNLO with FEWZ and three sets of PDFs. The cross sections in this table are calculated in the full phase space with 1% statistical precision. The theoretical predictions of the ratio R and its uncertainties are also given. "Other" contains uncertainties from EWK correction, scale dependence, and α_s.

Invariant mass	Cross section (pb)			$R\ (10^{-3})$	Uncertainties on R (%)	
bin (GeV)	CT10	CTEQ66	MSTW2008	MSTW2008	PDF	Other
15–20	787	811	819	812	+4.3/−3.3	+2.5/−2.7
20–30	476	483	499	494	+3.6/−2.8	+1.9/−3.6
30–40	135	137	142	141	+2.7/−2.3	+3.1/−2.1
40–50	53	54	56	55	+2.1/−1.9	+2.4/−2.5
50–60	27	27	29	28	+1.6/−1.5	+2.6/−2.0
60–76	32	32	33	33	+0.9/−0.9	+2.0/−2.4
76–86	56	57	58	58	+0.2/−0.2	+2.1/−2.5
86–96	822	825	852	844	+0.1/−0.1	+1.8/−2.2
96–106	51	51	53	52	+0.2/−0.2	+2.8/−2.0
106–120	12	12	13	13	+0.5/−0.5	+2.6/−2.2
120–150	6.7	6.7	7.0	6.9	+0.9/−0.9	+2.5/−1.7
150–200	2.6	2.6	2.7	2.7	+1.5/−1.6	+2.0/−1.8
200–600	1.3	1.3	1.3	1.3	+2.8/−2.9	+1.8/−2.1

to use the same T&P factors, derived from the same single-lepton p_T bins. Nevertheless, for the dimuon channel the efficiency uncertainty is at most 20% of the total uncertainty, significantly diluting the effect of these correlations in the final results. The resolution correlations, introduced through the unfolding procedure, only have a visible effect around the Z peak. In summary, the level of correlations does not affect the combination of results in a significant way.

Table 11 gives the measured shape r, defined in Eq. (11), both in the dimuon and dielectron channels and also the combined result. Figure 4 compares the measured (combined) results with the prediction from the FEWZ NNLO calculations, performed with the MSTW08 PDF set. To provide a meaningful comparison, each data point is located on the horizontal axis at the position where the theoretical function has a value equal to its mean value over the corresponding bin, following the procedure described in Ref. [31]. The measurements are very well reproduced by the theoretical calculations.

9 Summary

The Drell–Yan differential cross section normalized to the cross section in the Z region has been measured in pp collisions at $\sqrt{s} = 7$ TeV, in the dimuon and dielectron channels in the invariant mass range $15 < M(\ell\ell) < 600$ GeV. The measurement is based on event samples collected by the CMS experiment, corresponding to an integrated luminosity of 35.9 ± 1.4 pb^{-1}. Results are presented both inside the detector acceptance and in the full phase space, and the effect of final state QED radiation on the results is reported as well. A correct description of the measurements requires modeling to NNLO for dilepton invariant masses below about 30 GeV. The measurements are in good agreement with the NNLO theoretical predictions, as computed with FEWZ.

Table 11: Results for the DY spectrum normalized to the Z region and to the invariant mass bin width, using Eq. (11), before and after combining the two channels. The results presented are in GeV^{-1} units.

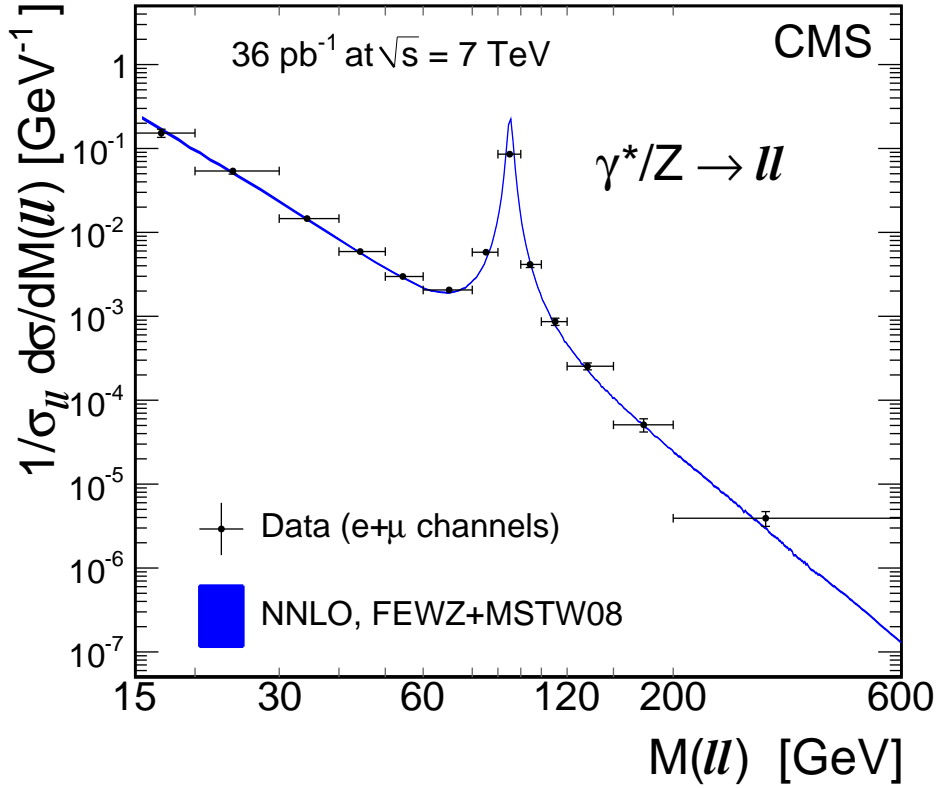| Invariant mass bin (GeV)	r (muons)	r (electrons)	r (combined)
15–20	$(15.6 \pm 1.4) \times 10^{-2}$	$(10.2 \pm 4.8) \times 10^{-2}$	$(15.2 \pm 1.3) \times 10^{-2}$
20–30	$(5.3 \pm 0.3) \times 10^{-2}$	$(5.6 \pm 1.0) \times 10^{-2}$	$(5.4 \pm 0.3) \times 10^{-2}$
30–40	$(1.5 \pm 0.1) \times 10^{-2}$	$(1.3 \pm 0.2) \times 10^{-2}$	$(1.5 \pm 0.1) \times 10^{-2}$
40–50	$(6.2 \pm 0.4) \times 10^{-3}$	$(4.7 \pm 0.7) \times 10^{-3}$	$(5.9 \pm 0.3) \times 10^{-3}$
50–60	$(3.0 \pm 0.2) \times 10^{-3}$	$(2.7 \pm 0.4) \times 10^{-3}$	$(3.0 \pm 0.2) \times 10^{-3}$
60–76	$(2.0 \pm 0.1) \times 10^{-3}$	$(2.2 \pm 0.3) \times 10^{-3}$	$(2.1 \pm 0.1) \times 10^{-3}$
76–86	$(5.8 \pm 0.3) \times 10^{-3}$	$(6.4 \pm 2.6) \times 10^{-3}$	$(5.8 \pm 0.3) \times 10^{-3}$
86–96	$(85.7 \pm 2.6) \times 10^{-3}$	$(83.4 \pm 6.0) \times 10^{-3}$	$(85.6 \pm 2.4) \times 10^{-3}$
96–106	$(4.1 \pm 0.3) \times 10^{-3}$	$(5.3 \pm 2.5) \times 10^{-3}$	$(4.2 \pm 0.3) \times 10^{-3}$
106–120	$(8.4 \pm 0.9) \times 10^{-4}$	$(9.6 \pm 1.9) \times 10^{-4}$	$(8.6 \pm 0.8) \times 10^{-4}$
120–150	$(2.9 \pm 0.3) \times 10^{-4}$	$(1.8 \pm 0.4) \times 10^{-4}$	$(2.5 \pm 0.2) \times 10^{-4}$
150–200	$(5.4 \pm 1.2) \times 10^{-5}$	$(4.6 \pm 1.4) \times 10^{-5}$	$(5.1 \pm 0.9) \times 10^{-5}$
200–600	$(3.7 \pm 1.0) \times 10^{-6}$	$(4.3 \pm 1.3) \times 10^{-6}$	$(3.9 \pm 0.8) \times 10^{-6}$

Acknowledgments

Figure 4:   DY invariant mass spectrum, normalized to the Z resonance region, $r =$ $(1/\sigma_{\ell\ell})d\sigma/dM(\ell\ell)$, as measured and as predicted by NNLO calculations, for the full phase space. The vertical error bar indicates the experimental (statistical and systematic) uncertainties summed in quadrature with the theory uncertainty resulting from the model-dependent kinematic distributions inside each bin. The horizontal bars indicate bin sizes and the data points inside are placed according to Ref. [31]. The width of the theory curve represents uncertainties from Table 10.

References

[1] K. Melnikov and F. Petriello, "Electroweak gauge boson production at hadron colliders through O(α_s^2)", *Phys. Rev. D* **74** (2006) 114017.
`doi:10.1103/PhysRevD.74.114017.`

[2] S. Catani, L. Cieri, G. Ferrera et al., "Vector boson production at hadron colliders: a fully exclusive QCD calculation at NNLO", *Phys. Rev. Lett.* **103** (2009) 082001.
`doi:10.1103/PhysRevLett.103.082001.`

[3] S. Catani and M. Grazzini, "An NNLO subtraction formalism in hadron collisions and its application to Higgs boson production at the LHC", *Phys. Rev. Lett.* **98** (2007) 222002.
`doi:10.1103/PhysRevLett.98.222002.`

[4] D0 Collaboration, "Measurement of the High-Mass Drell-Yan Cross Section and Limits on Quark-Electron Compositeness Scales", *Phys. Rev. Lett.* **82** (1999) 4769.
`doi:10.1103/PhysRevLett.82.4769.`

[5] CDF Collaboration, "Measurement of $d\sigma/dM$ and Forward-Backward Charge Asymmetry for High Mass Drell-Yan e^+e^- Pairs from p$\bar{\text{p}}$ Collisions at $\sqrt{s} = 1.8\,\text{TeV}$", *Phys. Rev. Lett.* **87** (2001) 131802. `doi:10.1103/PhysRevLett.87.131802.`

[6] CDF Collaboration, "Measurement of $d\sigma/dy$ of Drell-Yan e^+e^- pairs in the Z Mass Region from p$\bar{\text{p}}$ Collisions at $\sqrt{s} = 1.96\,\text{TeV}$", *Phys. Lett. B* **692** (2010) 232.
`doi:10.1016/j.physletb.2010.06.043.`

[7] CMS Collaboration, "Measurements of Inclusive W and Z Cross Sections in pp Collisions at $\sqrt{s} = 7\,\text{TeV}$", (2011). `arXiv:1107.4789.` Submitted to JHEP.

[8] CMS Collaboration, "The CMS experiment at the CERN LHC", *JINST* **3** (2008) S08004.
`doi:10.1088/1748-0221/3/08/S08004.`

[9] CMS Collaboration, "Performance of muon identification in pp collisions at $\sqrt{s} = 7\,\text{TeV}$", CMS Physics Analysis Summary CMS-PAS-MUO-10-002, (2010).

[10] CMS Collaboration, "Performance of CMS Muon Reconstruction in Cosmic-Ray Events", *JINST* **05** (2010) T03022. `doi:10.1088/1748-0221/5/03/T03022.`

[11] CMS Collaboration, "Electron Reconstruction and Identification at $\sqrt{s} = 7\,\text{TeV}$", CMS Physics Analysis Summary CMS-PAS-EGM-10-004, (2010).

[12] CMS Collaboration, "Measurement of the Lepton Charge Asymmetry in Inclusive W Production in pp Collisions at $\sqrt{s} = 7\,\text{TeV}$", *JHEP* **04** (2011) 050.
`doi:10.1007/JHEP04(2011)050.`

[13] S. Alioli, P. Nason, C. Oleari et al., "NLO vector-boson production matched with shower in POWHEG", *JHEP* **07** (2008) 060. `doi:10.1088/1126-6708/2008/07/060.`

[14] P. Nason, "A new method for combining NLO QCD with shower Monte Carlo algorithms", *JHEP* **11** (2004) 040. `doi:10.1088/1126-6708/2004/11/040.`

[15] S. Frixione, P. Nason, and C. Oleari, "Matching NLO QCD computations with Parton Shower simulations: the POWHEG method", *JHEP* **11** (2007) 070.
`doi:10.1088/1126-6708/2007/11/070.`

[16] T. Sjöstrand, S. Mrenna, and P. Z. Skands, "PYTHIA 6.4 Physics and Manual", *JHEP* **05** (2006) 026. `doi:10.1088/1126-6708/2006/05/026`.

[17] H. Lai et al., "New parton distributions for collider physics", *Phys. Rev. D* **82** (2010) 074024. `doi:10.1103/PhysRevD.82.074024`.

[18] J. Alwall, P. Demin, S. de Visscher et al., "MadGraph/MadEvent v4: the new web generation", *JHEP* **09** (2007) 028. `doi:10.1088/1126-6708/2007/09/028`.

[19] J. Pumplin et al., "New Generation of Parton Distributions with Uncertainties from Global Analysis", *JHEP* **07** (2002) 012. `doi:10.1088/1126-6708/2002/07/012`.

[20] S. Agostinelli et al., "GEANT4 - a simulation toolkit", *Nucl. Instr. and Methods A* **506** (2003) 250. `doi:10.1016/S0168-9002(03)01368-8`.

[21] CMS Collaboration, "Search for Resonances in the Dilepton Mass Distribution in pp Collisions at $\sqrt{s} = 7\,\text{TeV}$", *JHEP* **05** (2011) 093. `doi:10.1007/JHEP05(2011)093`.

[22] G. Cowan, "Statistical Data Analysis", ch. 11. Clarendon Press, Oxford, 1998.

[23] G. Bohm and G. Zech, "Introduction to Statistics and Data Analysis for Physicists", ch. 9. Verlag Deutsches Elektronen-Synchrotron, Hamburg, 1998.

[24] R. Gavin, Y. Li, P. Petriello et al., "FEWZ 2.0: A code for hadronic Z production at next-to-next-to-leading order", `arXiv:hep-ph/1011.3540`.

[25] D. Bourilkov, R. C. Group, and M. R. Whalley, "LHAPDF: PDF use from the Tevatron to the LHC", `arXiv:hep-ph/0605240`.

[26] P. M. Nadolsky et al., "Implications of CTEQ global analysis for collider observables", *Phys. Rev. D* **78** (2008) 013004. `doi:10.1103/PhysRevD.78.013004`.

[27] A. D. Martin et al., "Parton distributions for the LHC", *Eur. Phys. J. C* **63** (2009) 189. `doi:10.1140/epjc/s10052-009-1072-5`.

[28] D. Bourilkov, "Study of parton density function uncertainties with LHAPDF and PYTHIA at LHC", `arXiv:hep-ph/0305126`.

[29] M. R. Whalley, D. Bourilkov, and R. C. Group, "The Les Houches Accord PDFs (LHAPDF) and Lhaglue", `arXiv:hep-ph/0508110`.

[30] C. Calame, G. Montagna, O. Nicrosini et al., "Precision electroweak calculation of the production of a high transverse-momentum lepton pair at hadron colliders", *JHEP* **05** (2007) 109. `doi:10.1088/1126-6708/2007/10/109`.

[31] G. Lafferty and T. Wyatt, "Where to Stick Data Points: The Treatment of Measurements Within Wide Bins", *Nucl. Instr. and Methods A* **355** (1995) 541. `doi:10.1016/0168-9002(94)01112-5`.

A The CMS Collaboration

Yerevan Physics Institute, Yerevan, Armenia
S. Chatrchyan, V. Khachatryan, A.M. Sirunyan, A. Tumasyan

Institut für Hochenergiephysik der OeAW, Wien, Austria
W. Adam, T. Bergauer, M. Dragicevic, J. Erö, C. Fabjan, M. Friedl, R. Frühwirth, V.M. Ghete, J. Hammer[1], S. Hänsel, M. Hoch, N. Hörmann, J. Hrubec, M. Jeitler, W. Kiesenhofer, M. Krammer, D. Liko, I. Mikulec, M. Pernicka, B. Rahbaran, H. Rohringer, R. Schöfbeck, J. Strauss, A. Taurok, F. Teischinger, C. Trauner, P. Wagner, W. Waltenberger, G. Walzel, E. Widl, C.-E. Wulz

National Centre for Particle and High Energy Physics, Minsk, Belarus
V. Mossolov, N. Shumeiko, J. Suarez Gonzalez

Universiteit Antwerpen, Antwerpen, Belgium
S. Bansal, L. Benucci, E.A. De Wolf, X. Janssen, S. Luyckx, T. Maes, L. Mucibello, S. Ochesanu, B. Roland, R. Rougny, M. Selvaggi, H. Van Haevermaet, P. Van Mechelen, N. Van Remortel

Vrije Universiteit Brussel, Brussel, Belgium
F. Blekman, S. Blyweert, J. D'Hondt, R. Gonzalez Suarez, A. Kalogeropoulos, M. Maes, A. Olbrechts, W. Van Doninck, P. Van Mulders, G.P. Van Onsem, I. Villella

Université Libre de Bruxelles, Bruxelles, Belgium
O. Charaf, B. Clerbaux, G. De Lentdecker, V. Dero, A.P.R. Gay, G.H. Hammad, T. Hreus, P.E. Marage, A. Raval, L. Thomas, G. Vander Marcken, C. Vander Velde, P. Vanlaer

Ghent University, Ghent, Belgium
V. Adler, A. Cimmino, S. Costantini, M. Grunewald, B. Klein, J. Lellouch, A. Marinov, J. Mccartin, D. Ryckbosch, F. Thyssen, M. Tytgat, L. Vanelderen, P. Verwilligen, S. Walsh, N. Zaganidis

Université Catholique de Louvain, Louvain-la-Neuve, Belgium
S. Basegmez, G. Bruno, J. Caudron, L. Ceard, E. Cortina Gil, J. De Favereau De Jeneret, C. Delaere, D. Favart, A. Giammanco, G. Grégoire, J. Hollar, V. Lemaitre, J. Liao, O. Militaru, C. Nuttens, S. Ovyn, D. Pagano, A. Pin, K. Piotrzkowski, N. Schul

Université de Mons, Mons, Belgium
N. Beliy, T. Caebergs, E. Daubie

Centro Brasileiro de Pesquisas Fisicas, Rio de Janeiro, Brazil
G.A. Alves, L. Brito, D. De Jesus Damiao, M.E. Pol, M.H.G. Souza

Universidade do Estado do Rio de Janeiro, Rio de Janeiro, Brazil
W.L. Aldá Júnior, W. Carvalho, E.M. Da Costa, C. De Oliveira Martins, S. Fonseca De Souza, D. Matos Figueiredo, L. Mundim, H. Nogima, V. Oguri, W.L. Prado Da Silva, A. Santoro, S.M. Silva Do Amaral, A. Sznajder

Instituto de Fisica Teorica, Universidade Estadual Paulista, Sao Paulo, Brazil
C.A. Bernardes[2], F.A. Dias[3], T. Dos Anjos Costa[2], T.R. Fernandez Perez Tomei, E. M. Gregores[2], C. Lagana, F. Marinho, P.G. Mercadante[2], S.F. Novaes, Sandra S. Padula

Institute for Nuclear Research and Nuclear Energy, Sofia, Bulgaria
N. Darmenov[1], V. Genchev[1], P. Iaydjiev[1], S. Piperov, M. Rodozov, S. Stoykova, G. Sultanov, V. Tcholakov, R. Trayanov, M. Vutova

University of Sofia, Sofia, Bulgaria
A. Dimitrov, R. Hadjiiska, A. Karadzhinova, V. Kozhuharov, L. Litov, M. Mateev, B. Pavlov, P. Petkov

Institute of High Energy Physics, Beijing, China
J.G. Bian, G.M. Chen, H.S. Chen, C.H. Jiang, D. Liang, S. Liang, X. Meng, J. Tao, J. Wang, J. Wang, X. Wang, Z. Wang, H. Xiao, M. Xu, J. Zang, Z. Zhang

State Key Lab. of Nucl. Phys. and Tech., Peking University, Beijing, China
Y. Ban, S. Guo, Y. Guo, W. Li, Y. Mao, S.J. Qian, H. Teng, B. Zhu, W. Zou

Universidad de Los Andes, Bogota, Colombia
A. Cabrera, B. Gomez Moreno, A.A. Ocampo Rios, A.F. Osorio Oliveros, J.C. Sanabria

Technical University of Split, Split, Croatia
N. Godinovic, D. Lelas, K. Lelas, R. Plestina[4], D. Polic, I. Puljak

University of Split, Split, Croatia
Z. Antunovic, M. Dzelalija, M. Kovac

Institute Rudjer Boskovic, Zagreb, Croatia
V. Brigljevic, S. Duric, K. Kadija, J. Luetic, S. Morovic

University of Cyprus, Nicosia, Cyprus
A. Attikis, M. Galanti, J. Mousa, C. Nicolaou, F. Ptochos, P.A. Razis

Charles University, Prague, Czech Republic
M. Finger, M. Finger Jr.

Academy of Scientific Research and Technology of the Arab Republic of Egypt, Egyptian Network of High Energy Physics, Cairo, Egypt
Y. Assran[5], A. Ellithi Kamel, S. Khalil[6], M.A. Mahmoud[7], A. Radi[8]

National Institute of Chemical Physics and Biophysics, Tallinn, Estonia
A. Hektor, M. Kadastik, M. Müntel, M. Raidal, L. Rebane, A. Tiko

Department of Physics, University of Helsinki, Helsinki, Finland
V. Azzolini, P. Eerola, G. Fedi, M. Voutilainen

Helsinki Institute of Physics, Helsinki, Finland
S. Czellar, J. Härkönen, A. Heikkinen, V. Karimäki, R. Kinnunen, M.J. Kortelainen, T. Lampén, K. Lassila-Perini, S. Lehti, T. Lindén, P. Luukka, T. Mäenpää, E. Tuominen, J. Tuominiemi, E. Tuovinen, D. Ungaro, L. Wendland

Lappeenranta University of Technology, Lappeenranta, Finland
K. Banzuzi, A. Karjalainen, A. Korpela, T. Tuuva

Laboratoire d'Annecy-le-Vieux de Physique des Particules, IN2P3-CNRS, Annecy-le-Vieux, France
D. Sillou

DSM/IRFU, CEA/Saclay, Gif-sur-Yvette, France
M. Besancon, S. Choudhury, M. Dejardin, D. Denegri, B. Fabbro, J.L. Faure, F. Ferri, S. Ganjour, F.X. Gentit, A. Givernaud, P. Gras, G. Hamel de Monchenault, P. Jarry, E. Locci, J. Malcles, M. Marionneau, L. Millischer, J. Rander, A. Rosowsky, I. Shreyber, M. Titov, P. Verrecchia

Laboratoire Leprince-Ringuet, Ecole Polytechnique, IN2P3-CNRS, Palaiseau, France
S. Baffioni, F. Beaudette, L. Benhabib, L. Bianchini, M. Bluj[9], C. Broutin, P. Busson, C. Charlot, T. Dahms, L. Dobrzynski, S. Elgammal, R. Granier de Cassagnac, M. Haguenauer, P. Miné, C. Mironov, C. Ochando, P. Paganini, D. Sabes, R. Salerno, Y. Sirois, C. Thiebaux, C. Veelken, A. Zabi

Institut Pluridisciplinaire Hubert Curien, Université de Strasbourg, Université de Haute Alsace Mulhouse, CNRS/IN2P3, Strasbourg, France
J.-L. Agram[10], J. Andrea, D. Bloch, D. Bodin, J.-M. Brom, M. Cardaci, E.C. Chabert, C. Collard, E. Conte[10], F. Drouhin[10], C. Ferro, J.-C. Fontaine[10], D. Gelé, U. Goerlach, S. Greder, P. Juillot, M. Karim[10], A.-C. Le Bihan, Y. Mikami, P. Van Hove

Centre de Calcul de l'Institut National de Physique Nucleaire et de Physique des Particules (IN2P3), Villeurbanne, France
F. Fassi, D. Mercier

Université de Lyon, Université Claude Bernard Lyon 1, CNRS-IN2P3, Institut de Physique Nucléaire de Lyon, Villeurbanne, France
C. Baty, S. Beauceron, N. Beaupere, M. Bedjidian, O. Bondu, G. Boudoul, D. Boumediene, H. Brun, J. Chasserat, R. Chierici, D. Contardo, P. Depasse, H. El Mamouni, J. Fay, S. Gascon, B. Ille, T. Kurca, T. Le Grand, M. Lethuillier, L. Mirabito, S. Perries, V. Sordini, S. Tosi, Y. Tschudi, P. Verdier, S. Viret

Institute of High Energy Physics and Informatization, Tbilisi State University, Tbilisi, Georgia
D. Lomidze

RWTH Aachen University, I. Physikalisches Institut, Aachen, Germany
G. Anagnostou, S. Beranek, M. Edelhoff, L. Feld, N. Heracleous, O. Hindrichs, R. Jussen, K. Klein, J. Merz, N. Mohr, A. Ostapchuk, A. Perieanu, F. Raupach, J. Sammet, S. Schael, D. Sprenger, H. Weber, M. Weber, B. Wittmer, V. Zhukov[11]

RWTH Aachen University, III. Physikalisches Institut A, Aachen, Germany
M. Ata, E. Dietz-Laursonn, M. Erdmann, T. Hebbeker, C. Heidemann, A. Hinzmann, K. Hoepfner, T. Klimkovich, D. Klingebiel, P. Kreuzer, D. Lanske[†], J. Lingemann, C. Magass, M. Merschmeyer, A. Meyer, P. Papacz, H. Pieta, H. Reithler, S.A. Schmitz, L. Sonnenschein, J. Steggemann, D. Teyssier

RWTH Aachen University, III. Physikalisches Institut B, Aachen, Germany
M. Bontenackels, V. Cherepanov, M. Davids, G. Flügge, H. Geenen, M. Giffels, W. Haj Ahmad, F. Hoehle, B. Kargoll, T. Kress, Y. Kuessel, A. Linn, A. Nowack, L. Perchalla, O. Pooth, J. Rennefeld, P. Sauerland, A. Stahl, D. Tornier, M.H. Zoeller

Deutsches Elektronen-Synchrotron, Hamburg, Germany
M. Aldaya Martin, W. Behrenhoff, U. Behrens, M. Bergholz[12], A. Bethani, K. Borras, A. Cakir, A. Campbell, E. Castro, D. Dammann, G. Eckerlin, D. Eckstein, A. Flossdorf, G. Flucke, A. Geiser, J. Hauk, H. Jung[1], M. Kasemann, P. Katsas, C. Kleinwort, H. Kluge, A. Knutsson, M. Krämer, D. Krücker, E. Kuznetsova, W. Lange, W. Lohmann[12], R. Mankel, M. Marienfeld, I.-A. Melzer-Pellmann, A.B. Meyer, J. Mnich, A. Mussgiller, J. Olzem, A. Petrukhin, D. Pitzl, A. Raspereza, M. Rosin, R. Schmidt[12], T. Schoerner-Sadenius, N. Sen, A. Spiridonov, M. Stein, J. Tomaszewska, R. Walsh, C. Wissing

University of Hamburg, Hamburg, Germany
C. Autermann, V. Blobel, S. Bobrovskyi, J. Draeger, H. Enderle, U. Gebbert, M. Görner,

T. Hermanns, K. Kaschube, G. Kaussen, H. Kirschenmann, R. Klanner, J. Lange, B. Mura, S. Naumann-Emme, F. Nowak, N. Pietsch, C. Sander, H. Schettler, P. Schleper, E. Schlieckau, M. Schröder, T. Schum, H. Stadie, G. Steinbrück, J. Thomsen

Institut für Experimentelle Kernphysik, Karlsruhe, Germany
C. Barth, J. Bauer, J. Berger, V. Buege, T. Chwalek, W. De Boer, A. Dierlamm, G. Dirkes, M. Feindt, J. Gruschke, C. Hackstein, F. Hartmann, M. Heinrich, H. Held, K.H. Hoffmann, S. Honc, I. Katkov[11], J.R. Komaragiri, T. Kuhr, D. Martschei, S. Mueller, Th. Müller, M. Niegel, O. Oberst, A. Oehler, J. Ott, T. Peiffer, G. Quast, K. Rabbertz, F. Ratnikov, N. Ratnikova, M. Renz, S. Röcker, C. Saout, A. Scheurer, P. Schieferdecker, F.-P. Schilling, M. Schmanau, G. Schott, H.J. Simonis, F.M. Stober, D. Troendle, J. Wagner-Kuhr, T. Weiler, M. Zeise, E.B. Ziebarth

Institute of Nuclear Physics ”Demokritos”, Aghia Paraskevi, Greece
G. Daskalakis, T. Geralis, S. Kesisoglou, A. Kyriakis, D. Loukas, I. Manolakos, A. Markou, C. Markou, C. Mavrommatis, E. Ntomari, E. Petrakou

University of Athens, Athens, Greece
L. Gouskos, T.J. Mertzimekis, A. Panagiotou, N. Saoulidou, E. Stiliaris

University of Ioánnina, Ioánnina, Greece
I. Evangelou, C. Foudas[1], P. Kokkas, N. Manthos, I. Papadopoulos, V. Patras, F.A. Triantis

KFKI Research Institute for Particle and Nuclear Physics, Budapest, Hungary
A. Aranyi, G. Bencze, L. Boldizsar, C. Hajdu[1], P. Hidas, D. Horvath[13], A. Kapusi, K. Krajczar[14], F. Sikler[1], G.I. Veres[14], G. Vesztergombi[14]

Institute of Nuclear Research ATOMKI, Debrecen, Hungary
N. Beni, J. Molnar, J. Palinkas, Z. Szillasi, V. Veszpremi

University of Debrecen, Debrecen, Hungary
J. Karancsi, P. Raics, Z.L. Trocsanyi, B. Ujvari

Panjab University, Chandigarh, India
S.B. Beri, V. Bhatnagar, N. Dhingra, R. Gupta, M. Jindal, M. Kaur, J.M. Kohli, M.Z. Mehta, N. Nishu, L.K. Saini, A. Sharma, A.P. Singh, J. Singh, S.P. Singh

University of Delhi, Delhi, India
S. Ahuja, B.C. Choudhary, P. Gupta, A. Kumar, A. Kumar, S. Malhotra, M. Naimuddin, K. Ranjan, R.K. Shivpuri

Saha Institute of Nuclear Physics, Kolkata, India
S. Banerjee, S. Bhattacharya, S. Dutta, B. Gomber, S. Jain, S. Jain, R. Khurana, S. Sarkar

Bhabha Atomic Research Centre, Mumbai, India
R.K. Choudhury, D. Dutta, S. Kailas, V. Kumar, P. Mehta, A.K. Mohanty[1], L.M. Pant, P. Shukla

Tata Institute of Fundamental Research - EHEP, Mumbai, India
T. Aziz, M. Guchait[15], A. Gurtu, M. Maity[16], D. Majumder, G. Majumder, T. Mathew, K. Mazumdar, G.B. Mohanty, A. Saha, K. Sudhakar, N. Wickramage

Tata Institute of Fundamental Research - HECR, Mumbai, India
S. Banerjee, S. Dugad, N.K. Mondal

Institute for Research and Fundamental Sciences (IPM), Tehran, Iran
H. Arfaei, H. Bakhshiansohi[17], S.M. Etesami[18], A. Fahim[17], M. Hashemi, H. Hesari, A. Jafari[17],

M. Khakzad, A. Mohammadi[19], M. Mohammadi Najafabadi, S. Paktinat Mehdiabadi, B. Safarzadeh, M. Zeinali[18]

INFN Sezione di Bari [a], Università di Bari [b], Politecnico di Bari [c], Bari, Italy
M. Abbrescia[a,b], L. Barbone[a,b], C. Calabria[a,b], A. Colaleo[a], D. Creanza[a,c], N. De Filippis[a,c,1], M. De Palma[a,b], L. Fiore[a], G. Iaselli[a,c], L. Lusito[a,b], G. Maggi[a,c], M. Maggi[a], N. Manna[a,b], B. Marangelli[a,b], S. My[a,c], S. Nuzzo[a,b], N. Pacifico[a,b], G.A. Pierro[a], A. Pompili[a,b], G. Pugliese[a,c], F. Romano[a,c], G. Roselli[a,b], G. Selvaggi[a,b], L. Silvestris[a], R. Trentadue[a], S. Tupputi[a,b], G. Zito[a]

INFN Sezione di Bologna [a], Università di Bologna [b], Bologna, Italy
G. Abbiendi[a], A.C. Benvenuti[a], D. Bonacorsi[a], S. Braibant-Giacomelli[a,b], L. Brigliadori[a], P. Capiluppi[a,b], A. Castro[a,b], F.R. Cavallo[a], M. Cuffiani[a,b], G.M. Dallavalle[a], F. Fabbri[a], A. Fanfani[a,b], D. Fasanella[a,1], P. Giacomelli[a], M. Giunta[a], C. Grandi[a], S. Marcellini[a], G. Masetti[b], M. Meneghelli[a,b], A. Montanari[a], F.L. Navarria[a,b], F. Odorici[a], A. Perrotta[a], F. Primavera[a], A.M. Rossi[a,b], T. Rovelli[a,b], G. Siroli[a,b], R. Travaglini[a,b]

INFN Sezione di Catania [a], Università di Catania [b], Catania, Italy
S. Albergo[a,b], G. Cappello[a,b], M. Chiorboli[a,b], S. Costa[a,b], R. Potenza[a,b], A. Tricomi[a,b], C. Tuve[a,b]

INFN Sezione di Firenze [a], Università di Firenze [b], Firenze, Italy
G. Barbagli[a], V. Ciulli[a,b], C. Civinini[a], R. D'Alessandro[a,b], E. Focardi[a,b], S. Frosali[a,b], E. Gallo[a], S. Gonzi[a,b], P. Lenzi[a,b], M. Meschini[a], S. Paoletti[a], G. Sguazzoni[a], A. Tropiano[a,1]

INFN Laboratori Nazionali di Frascati, Frascati, Italy
L. Benussi, S. Bianco, S. Colafranceschi[20], F. Fabbri, D. Piccolo

INFN Sezione di Genova, Genova, Italy
P. Fabbricatore, R. Musenich

INFN Sezione di Milano-Bicocca [a], Università di Milano-Bicocca [b], Milano, Italy
A. Benaglia[a,b,1], F. De Guio[a,b], L. Di Matteo[a,b], S. Gennai[1], A. Ghezzi[a,b], S. Malvezzi[a], A. Martelli[a,b], A. Massironi[a,b,1], D. Menasce[a], L. Moroni[a], M. Paganoni[a,b], D. Pedrini[a], S. Ragazzi[a,b], N. Redaelli[a], S. Sala[a], T. Tabarelli de Fatis[a,b]

INFN Sezione di Napoli [a], Università di Napoli "Federico II" [b], Napoli, Italy
S. Buontempo[a], C.A. Carrillo Montoya[a,1], N. Cavallo[a,21], A. De Cosa[a,b], F. Fabozzi[a,21], A.O.M. Iorio[a,1], L. Lista[a], M. Merola[a,b], P. Paolucci[a]

INFN Sezione di Padova [a], Università di Padova [b], Università di Trento (Trento) [c], Padova, Italy
P. Azzi[a], N. Bacchetta[a,1], P. Bellan[a,b], D. Bisello[a,b], A. Branca[a], R. Carlin[a,b], P. Checchia[a], T. Dorigo[a], U. Dosselli[a], F. Fanzago[a], F. Gasparini[a,b], U. Gasparini[a,b], A. Gozzelino, S. Lacaprara[a,22], I. Lazzizzera[a,c], M. Margoni[a,b], M. Mazzucato[a], A.T. Meneguzzo[a,b], M. Nespolo[a,1], L. Perrozzi[a], N. Pozzobon[a,b], P. Ronchese[a,b], F. Simonetto[a,b], E. Torassa[a], M. Tosi[a,b,1], S. Vanini[a,b], P. Zotto[a,b], G. Zumerle[a,b]

INFN Sezione di Pavia [a], Università di Pavia [b], Pavia, Italy
P. Baesso[a,b], U. Berzano[a], S.P. Ratti[a,b], C. Riccardi[a,b], P. Torre[a,b], P. Vitulo[a,b], C. Viviani[a,b]

INFN Sezione di Perugia [a], Università di Perugia [b], Perugia, Italy
M. Biasini[a,b], G.M. Bilei[a], B. Caponeri[a,b], L. Fanò[a,b], P. Lariccia[a,b], A. Lucaroni[a,b,1], G. Mantovani[a,b], M. Menichelli[a], A. Nappi[a,b], F. Romeo[a,b], A. Santocchia[a,b], S. Taroni[a,b,1], M. Valdata[a,b]

INFN Sezione di Pisa [a]**, Università di Pisa** [b]**, Scuola Normale Superiore di Pisa** [c]**, Pisa, Italy**
P. Azzurri[a,c], G. Bagliesi[a], J. Bernardini[a,b], T. Boccali[a], G. Broccolo[a,c], R. Castaldi[a], R.T. D'Agnolo[a,c], R. Dell'Orso[a], F. Fiori[a,b], L. Foà[a,c], A. Giassi[a], A. Kraan[a], F. Ligabue[a,c], T. Lomtadze[a], L. Martini[a,23], A. Messineo[a,b], F. Palla[a], F. Palmonari, G. Segneri[a], A.T. Serban[a], P. Spagnolo[a], R. Tenchini[a], G. Tonelli[a,b,1], A. Venturi[a,1], P.G. Verdini[a]

INFN Sezione di Roma [a]**, Università di Roma "La Sapienza"** [b]**, Roma, Italy**
L. Barone[a,b], F. Cavallari[a], D. Del Re[a,b,1], E. Di Marco[a,b], M. Diemoz[a], D. Franci[a,b], M. Grassi[a,1], E. Longo[a,b], P. Meridiani, S. Nourbakhsh[a], G. Organtini[a,b], F. Pandolfi[a,b], R. Paramatti[a], S. Rahatlou[a,b], M. Sigamani[a]

INFN Sezione di Torino [a]**, Università di Torino** [b]**, Università del Piemonte Orientale (Novara)** [c]**, Torino, Italy**
N. Amapane[a,b], R. Arcidiacono[a,c], S. Argiro[a,b], M. Arneodo[a,c], C. Biino[a], C. Botta[a,b], N. Cartiglia[a], R. Castello[a,b], M. Costa[a,b], N. Demaria[a], A. Graziano[a,b], C. Mariotti[a], S. Maselli[a], E. Migliore[a,b], V. Monaco[a,b], M. Musich[a], M.M. Obertino[a,c], N. Pastrone[a], M. Pelliccioni[a,b], A. Potenza[a,b], A. Romero[a,b], M. Ruspa[a,c], R. Sacchi[a,b], V. Sola[a,b], A. Solano[a,b], A. Staiano[a], A. Vilela Pereira[a]

INFN Sezione di Trieste [a]**, Università di Trieste** [b]**, Trieste, Italy**
S. Belforte[a], F. Cossutti[a], G. Della Ricca[a,b], B. Gobbo[a], M. Marone[a,b], D. Montanino[a,b], A. Penzo[a]

Kangwon National University, Chunchon, Korea
S.G. Heo, S.K. Nam

Kyungpook National University, Daegu, Korea
S. Chang, J. Chung, D.H. Kim, G.N. Kim, J.E. Kim, D.J. Kong, H. Park, S.R. Ro, D.C. Son, T. Son

Chonnam National University, Institute for Universe and Elementary Particles, Kwangju, Korea
J.Y. Kim, Zero J. Kim, S. Song

Konkuk University, Seoul, Korea
H.Y. Jo

Korea University, Seoul, Korea
S. Choi, D. Gyun, B. Hong, M. Jo, H. Kim, J.H. Kim, T.J. Kim, K.S. Lee, D.H. Moon, S.K. Park, E. Seo, K.S. Sim

University of Seoul, Seoul, Korea
M. Choi, S. Kang, H. Kim, C. Park, I.C. Park, S. Park, G. Ryu

Sungkyunkwan University, Suwon, Korea
Y. Cho, Y. Choi, Y.K. Choi, J. Goh, M.S. Kim, B. Lee, J. Lee, S. Lee, H. Seo, I. Yu

Vilnius University, Vilnius, Lithuania
M.J. Bilinskas, I. Grigelionis, M. Janulis, D. Martisiute, P. Petrov, M. Polujanskas, T. Sabonis

Centro de Investigacion y de Estudios Avanzados del IPN, Mexico City, Mexico
H. Castilla-Valdez, E. De La Cruz-Burelo, I. Heredia-de La Cruz, R. Lopez-Fernandez, R. Magaña Villalba, J. Martínez-Ortega, A. Sánchez-Hernández, L.M. Villasenor-Cendejas

Universidad Iberoamericana, Mexico City, Mexico
S. Carrillo Moreno, F. Vazquez Valencia

Benemerita Universidad Autonoma de Puebla, Puebla, Mexico
H.A. Salazar Ibarguen

Universidad Autónoma de San Luis Potosí, San Luis Potosí, Mexico
E. Casimiro Linares, A. Morelos Pineda, M.A. Reyes-Santos

University of Auckland, Auckland, New Zealand
D. Krofcheck, J. Tam

University of Canterbury, Christchurch, New Zealand
P.H. Butler, R. Doesburg, H. Silverwood

National Centre for Physics, Quaid-I-Azam University, Islamabad, Pakistan
M. Ahmad, I. Ahmed, M.H. Ansari, M.I. Asghar, H.R. Hoorani, S. Khalid, W.A. Khan, T. Khurshid, S. Qazi, M.A. Shah, M. Shoaib

Institute of Experimental Physics, Faculty of Physics, University of Warsaw, Warsaw, Poland
G. Brona, M. Cwiok, W. Dominik, K. Doroba, A. Kalinowski, M. Konecki, J. Krolikowski

Soltan Institute for Nuclear Studies, Warsaw, Poland
T. Frueboes, R. Gokieli, M. Górski, M. Kazana, K. Nawrocki, K. Romanowska-Rybinska, M. Szleper, G. Wrochna, P. Zalewski

Laboratório de Instrumentação e Física Experimental de Partículas, Lisboa, Portugal
N. Almeida, P. Bargassa, A. David, P. Faccioli, P.G. Ferreira Parracho, M. Gallinaro[1], P. Musella, A. Nayak, J. Pela[1], P.Q. Ribeiro, J. Seixas, J. Varela

Joint Institute for Nuclear Research, Dubna, Russia
S. Afanasiev, I. Belotelov, P. Bunin, M. Gavrilenko, I. Golutvin, A. Kamenev, V. Karjavin, G. Kozlov, A. Lanev, P. Moisenz, V. Palichik, V. Perelygin, S. Shmatov, V. Smirnov, A. Volodko, A. Zarubin

Petersburg Nuclear Physics Institute, Gatchina (St Petersburg), Russia
V. Golovtsov, Y. Ivanov, V. Kim, P. Levchenko, V. Murzin, V. Oreshkin, I. Smirnov, V. Sulimov, L. Uvarov, S. Vavilov, A. Vorobyev, An. Vorobyev

Institute for Nuclear Research, Moscow, Russia
Yu. Andreev, A. Dermenev, S. Gninenko, N. Golubev, M. Kirsanov, N. Krasnikov, V. Matveev, A. Pashenkov, A. Toropin, S. Troitsky

Institute for Theoretical and Experimental Physics, Moscow, Russia
V. Epshteyn, M. Erofeeva, V. Gavrilov, V. Kaftanov[†], M. Kossov[1], A. Krokhotin, N. Lychkovskaya, V. Popov, G. Safronov, S. Semenov, V. Stolin, E. Vlasov, A. Zhokin

Moscow State University, Moscow, Russia
A. Belyaev, E. Boos, M. Dubinin[3], L. Dudko, A. Ershov, A. Gribushin, O. Kodolova, I. Lokhtin, A. Markina, S. Obraztsov, M. Perfilov, S. Petrushanko, L. Sarycheva, V. Savrin, A. Snigirev

P.N. Lebedev Physical Institute, Moscow, Russia
V. Andreev, M. Azarkin, I. Dremin, M. Kirakosyan, A. Leonidov, G. Mesyats, S.V. Rusakov, A. Vinogradov

State Research Center of Russian Federation, Institute for High Energy Physics, Protvino, Russia
I. Azhgirey, I. Bayshev, S. Bitioukov, V. Grishin[1], V. Kachanov, D. Konstantinov, A. Korablev,

V. Krychkine, V. Petrov, R. Ryutin, A. Sobol, L. Tourtchanovitch, S. Troshin, N. Tyurin, A. Uzunian, A. Volkov

University of Belgrade, Faculty of Physics and Vinca Institute of Nuclear Sciences, Belgrade, Serbia
P. Adzic[24], M. Djordjevic, D. Krpic[24], J. Milosevic

Centro de Investigaciones Energéticas Medioambientales y Tecnológicas (CIEMAT), Madrid, Spain
M. Aguilar-Benitez, J. Alcaraz Maestre, P. Arce, C. Battilana, E. Calvo, M. Cerrada, M. Chamizo Llatas, N. Colino, B. De La Cruz, A. Delgado Peris, C. Diez Pardos, D. Domínguez Vázquez, C. Fernandez Bedoya, J.P. Fernández Ramos, A. Ferrando, J. Flix, M.C. Fouz, P. Garcia-Abia, O. Gonzalez Lopez, S. Goy Lopez, J.M. Hernandez, M.I. Josa, G. Merino, J. Puerta Pelayo, I. Redondo, L. Romero, J. Santaolalla, M.S. Soares, C. Willmott

Universidad Autónoma de Madrid, Madrid, Spain
C. Albajar, G. Codispoti, J.F. de Trocóniz

Universidad de Oviedo, Oviedo, Spain
J. Cuevas, J. Fernandez Menendez, S. Folgueras, I. Gonzalez Caballero, L. Lloret Iglesias, J.M. Vizan Garcia

Instituto de Física de Cantabria (IFCA), CSIC-Universidad de Cantabria, Santander, Spain
J.A. Brochero Cifuentes, I.J. Cabrillo, A. Calderon, S.H. Chuang, J. Duarte Campderros, M. Felcini[25], M. Fernandez, G. Gomez, J. Gonzalez Sanchez, C. Jorda, P. Lobelle Pardo, A. Lopez Virto, J. Marco, R. Marco, C. Martinez Rivero, F. Matorras, F.J. Munoz Sanchez, J. Piedra Gomez[26], T. Rodrigo, A.Y. Rodríguez-Marrero, A. Ruiz-Jimeno, L. Scodellaro, M. Sobron Sanudo, I. Vila, R. Vilar Cortabitarte

CERN, European Organization for Nuclear Research, Geneva, Switzerland
D. Abbaneo, E. Auffray, G. Auzinger, P. Baillon, A.H. Ball, D. Barney, A.J. Bell[27], D. Benedetti, C. Bernet[4], W. Bialas, P. Bloch, A. Bocci, S. Bolognesi, M. Bona, H. Breuker, K. Bunkowski, T. Camporesi, G. Cerminara, T. Christiansen, J.A. Coarasa Perez, B. Curé, D. D'Enterria, A. De Roeck, S. Di Guida, N. Dupont-Sagorin, A. Elliott-Peisert, B. Frisch, W. Funk, A. Gaddi, G. Georgiou, H. Gerwig, D. Gigi, K. Gill, D. Giordano, F. Glege, R. Gomez-Reino Garrido, M. Gouzevitch, P. Govoni, S. Gowdy, R. Guida, L. Guiducci, M. Hansen, C. Hartl, J. Harvey, J. Hegeman, B. Hegner, H.F. Hoffmann, V. Innocente, P. Janot, K. Kaadze, E. Karavakis, P. Lecoq, C. Lourenço, T. Mäki, M. Malberti, L. Malgeri, M. Mannelli, L. Masetti, A. Maurisset, F. Meijers, S. Mersi, E. Meschi, R. Moser, M.U. Mozer, M. Mulders, E. Nesvold, M. Nguyen, T. Orimoto, L. Orsini, E. Palencia Cortezon, E. Perez, A. Petrilli, A. Pfeiffer, M. Pierini, M. Pimiä, D. Piparo, G. Polese, L. Quertenmont, A. Racz, W. Reece, J. Rodrigues Antunes, G. Rolandi[28], T. Rommerskirchen, C. Rovelli[29], M. Rovere, H. Sakulin, C. Schäfer, C. Schwick, I. Segoni, A. Sharma, P. Siegrist, P. Silva, M. Simon, P. Sphicas[30], D. Spiga, M. Spiropulu[3], M. Stoye, A. Tsirou, P. Vichoudis, H.K. Wöhri, S.D. Worm, W.D. Zeuner

Paul Scherrer Institut, Villigen, Switzerland
W. Bertl, K. Deiters, W. Erdmann, K. Gabathuler, R. Horisberger, Q. Ingram, H.C. Kaestli, S. König, D. Kotlinski, U. Langenegger, F. Meier, D. Renker, T. Rohe, J. Sibille[31]

Institute for Particle Physics, ETH Zurich, Zurich, Switzerland
L. Bäni, P. Bortignon, L. Caminada[32], B. Casal, N. Chanon, Z. Chen, S. Cittolin, G. Dissertori, M. Dittmar, J. Eugster, K. Freudenreich, C. Grab, W. Hintz, P. Lecomte, W. Lustermann, C. Marchica[32], P. Martinez Ruiz del Arbol, P. Milenovic[33], F. Moortgat, C. Nägeli[32], P. Nef,

F. Nessi-Tedaldi, L. Pape, F. Pauss, T. Punz, A. Rizzi, F.J. Ronga, M. Rossini, L. Sala, A.K. Sanchez, M.-C. Sawley, A. Starodumov[34], B. Stieger, M. Takahashi, L. Tauscher[†], A. Thea, K. Theofilatos, D. Treille, C. Urscheler, R. Wallny, M. Weber, L. Wehrli, J. Weng

Universität Zürich, Zurich, Switzerland
E. Aguilo, C. Amsler, V. Chiochia, S. De Visscher, C. Favaro, M. Ivova Rikova, A. Jaeger, B. Millan Mejias, P. Otiougova, P. Robmann, A. Schmidt, H. Snoek

National Central University, Chung-Li, Taiwan
Y.H. Chang, K.H. Chen, C.M. Kuo, S.W. Li, W. Lin, Z.K. Liu, Y.J. Lu, D. Mekterovic, R. Volpe, S.S. Yu

National Taiwan University (NTU), Taipei, Taiwan
P. Bartalini, P. Chang, Y.H. Chang, Y.W. Chang, Y. Chao, K.F. Chen, C. Dietz, W.-S. Hou, Y. Hsiung, K.Y. Kao, Y.J. Lei, R.-S. Lu, J.G. Shiu, Y.M. Tzeng, X. Wan, M. Wang

Cukurova University, Adana, Turkey
A. Adiguzel, M.N. Bakirci[35], S. Cerci[36], C. Dozen, I. Dumanoglu, E. Eskut, S. Girgis, G. Gokbulut, I. Hos, E.E. Kangal, A. Kayis Topaksu, G. Onengut, K. Ozdemir, S. Ozturk[37], A. Polatoz, K. Sogut[38], D. Sunar Cerci[36], B. Tali[36], H. Topakli[35], D. Uzun, L.N. Vergili, M. Vergili

Middle East Technical University, Physics Department, Ankara, Turkey
I.V. Akin, T. Aliev, B. Bilin, S. Bilmis, M. Deniz, H. Gamsizkan, A.M. Guler, K. Ocalan, A. Ozpineci, M. Serin, R. Sever, U.E. Surat, M. Yalvac, E. Yildirim, M. Zeyrek

Bogazici University, Istanbul, Turkey
M. Deliomeroglu, D. Demir[39], E. Gülmez, B. Isildak, M. Kaya[40], O. Kaya[40], M. Özbek, S. Ozkorucuklu[41], N. Sonmez[42]

National Scientific Center, Kharkov Institute of Physics and Technology, Kharkov, Ukraine
L. Levchuk

University of Bristol, Bristol, United Kingdom
F. Bostock, J.J. Brooke, T.L. Cheng, E. Clement, D. Cussans, R. Frazier, J. Goldstein, M. Grimes, D. Hartley, G.P. Heath, H.F. Heath, L. Kreczko, S. Metson, D.M. Newbold[43], K. Nirunpong, A. Poll, S. Senkin, V.J. Smith

Rutherford Appleton Laboratory, Didcot, United Kingdom
L. Basso[44], K.W. Bell, A. Belyaev[44], C. Brew, R.M. Brown, B. Camanzi, D.J.A. Cockerill, J.A. Coughlan, K. Harder, S. Harper, J. Jackson, B.W. Kennedy, E. Olaiya, D. Petyt, B.C. Radburn-Smith, C.H. Shepherd-Themistocleous, I.R. Tomalin, W.J. Womersley

Imperial College, London, United Kingdom
R. Bainbridge, G. Ball, J. Ballin, R. Beuselinck, O. Buchmuller, D. Colling, N. Cripps, M. Cutajar, G. Davies, M. Della Negra, W. Ferguson, J. Fulcher, D. Futyan, A. Gilbert, A. Guneratne Bryer, G. Hall, Z. Hatherell, J. Hays, G. Iles, M. Jarvis, G. Karapostoli, L. Lyons, A.-M. Magnan, J. Marrouche, B. Mathias, R. Nandi, J. Nash, A. Nikitenko[34], A. Papageorgiou, M. Pesaresi, K. Petridis, M. Pioppi[45], D.M. Raymond, S. Rogerson, N. Rompotis, A. Rose, M.J. Ryan, C. Seez, P. Sharp, A. Sparrow, A. Tapper, S. Tourneur, M. Vazquez Acosta, T. Virdee, S. Wakefield, N. Wardle, D. Wardrope, T. Whyntie

Brunel University, Uxbridge, United Kingdom
M. Barrett, M. Chadwick, J.E. Cole, P.R. Hobson, A. Khan, P. Kyberd, D. Leslie, W. Martin, I.D. Reid, L. Teodorescu

Baylor University, Waco, USA
K. Hatakeyama, H. Liu

The University of Alabama, Tuscaloosa, USA
C. Henderson

Boston University, Boston, USA
T. Bose, E. Carrera Jarrin, C. Fantasia, A. Heister, J. St. John, P. Lawson, D. Lazic, J. Rohlf, D. Sperka, L. Sulak

Brown University, Providence, USA
A. Avetisyan, S. Bhattacharya, J.P. Chou, D. Cutts, A. Ferapontov, U. Heintz, S. Jabeen, G. Kukartsev, G. Landsberg, M. Luk, M. Narain, D. Nguyen, M. Segala, T. Sinthuprasith, T. Speer, K.V. Tsang

University of California, Davis, Davis, USA
R. Breedon, G. Breto, M. Calderon De La Barca Sanchez, S. Chauhan, M. Chertok, J. Conway, R. Conway, P.T. Cox, J. Dolen, R. Erbacher, R. Houtz, W. Ko, A. Kopecky, R. Lander, H. Liu, O. Mall, S. Maruyama, T. Miceli, M. Nikolic, D. Pellett, J. Robles, B. Rutherford, S. Salur, M. Searle, J. Smith, M. Squires, M. Tripathi, R. Vasquez Sierra

University of California, Los Angeles, Los Angeles, USA
V. Andreev, K. Arisaka, D. Cline, R. Cousins, A. Deisher, J. Duris, S. Erhan, C. Farrell, J. Hauser, M. Ignatenko, C. Jarvis, C. Plager, G. Rakness, P. Schlein[†], J. Tucker, V. Valuev

University of California, Riverside, Riverside, USA
J. Babb, R. Clare, J. Ellison, J.W. Gary, F. Giordano, G. Hanson, G.Y. Jeng, S.C. Kao, H. Liu, O.R. Long, A. Luthra, H. Nguyen, S. Paramesvaran, J. Sturdy, S. Sumowidagdo, R. Wilken, S. Wimpenny

University of California, San Diego, La Jolla, USA
W. Andrews, J.G. Branson, G.B. Cerati, D. Evans, F. Golf, A. Holzner, R. Kelley, M. Lebourgeois, J. Letts, B. Mangano, S. Padhi, C. Palmer, G. Petrucciani, H. Pi, M. Pieri, R. Ranieri, M. Sani, V. Sharma, S. Simon, E. Sudano, M. Tadel, Y. Tu, A. Vartak, S. Wasserbaech[46], F. Würthwein, A. Yagil, J. Yoo

University of California, Santa Barbara, Santa Barbara, USA
D. Barge, R. Bellan, C. Campagnari, M. D'Alfonso, T. Danielson, K. Flowers, P. Geffert, J. Incandela, C. Justus, P. Kalavase, S.A. Koay, D. Kovalskyi[1], V. Krutelyov, S. Lowette, N. Mccoll, S.D. Mullin, V. Pavlunin, F. Rebassoo, J. Ribnik, J. Richman, R. Rossin, D. Stuart, W. To, J.R. Vlimant, C. West

California Institute of Technology, Pasadena, USA
A. Apresyan, A. Bornheim, J. Bunn, Y. Chen, J. Duarte, M. Gataullin, Y. Ma, A. Mott, H.B. Newman, C. Rogan, K. Shin, V. Timciuc, P. Traczyk, J. Veverka, R. Wilkinson, Y. Yang, R.Y. Zhu

Carnegie Mellon University, Pittsburgh, USA
B. Akgun, R. Carroll, T. Ferguson, Y. Iiyama, D.W. Jang, S.Y. Jun, Y.F. Liu, M. Paulini, J. Russ, H. Vogel, I. Vorobiev

University of Colorado at Boulder, Boulder, USA
J.P. Cumalat, M.E. Dinardo, B.R. Drell, C.J. Edelmaier, W.T. Ford, A. Gaz, B. Heyburn, E. Luiggi Lopez, U. Nauenberg, J.G. Smith, K. Stenson, K.A. Ulmer, S.R. Wagner, S.L. Zang

Cornell University, Ithaca, USA
L. Agostino, J. Alexander, A. Chatterjee, N. Eggert, L.K. Gibbons, B. Heltsley, W. Hopkins, A. Khukhunaishvili, B. Kreis, G. Nicolas Kaufman, J.R. Patterson, D. Puigh, A. Ryd, E. Salvati, X. Shi, W. Sun, W.D. Teo, J. Thom, J. Thompson, J. Vaughan, Y. Weng, L. Winstrom, P. Wittich

Fairfield University, Fairfield, USA
A. Biselli, G. Cirino, D. Winn

Fermi National Accelerator Laboratory, Batavia, USA
S. Abdullin, M. Albrow, J. Anderson, G. Apollinari, M. Atac, J.A. Bakken, L.A.T. Bauerdick, A. Beretvas, J. Berryhill, P.C. Bhat, I. Bloch, K. Burkett, J.N. Butler, V. Chetluru, H.W.K. Cheung, F. Chlebana, S. Cihangir, W. Cooper, D.P. Eartly, V.D. Elvira, S. Esen, I. Fisk, J. Freeman, Y. Gao, E. Gottschalk, D. Green, K. Gunthoti, O. Gutsche, J. Hanlon, R.M. Harris, J. Hirschauer, B. Hooberman, H. Jensen, S. Jindariani, M. Johnson, U. Joshi, R. Khatiwada, B. Klima, K. Kousouris, S. Kunori, S. Kwan, C. Leonidopoulos, P. Limon, D. Lincoln, R. Lipton, J. Lykken, K. Maeshima, J.M. Marraffino, D. Mason, P. McBride, T. Miao, K. Mishra, S. Mrenna, Y. Musienko[47], C. Newman-Holmes, V. O'Dell, J. Pivarski, R. Pordes, O. Prokofyev, T. Schwarz, E. Sexton-Kennedy, S. Sharma, W.J. Spalding, L. Spiegel, P. Tan, L. Taylor, S. Tkaczyk, L. Uplegger, E.W. Vaandering, R. Vidal, J. Whitmore, W. Wu, F. Yang, F. Yumiceva, J.C. Yun

University of Florida, Gainesville, USA
D. Acosta, P. Avery, D. Bourilkov, M. Chen, S. Das, M. De Gruttola, G.P. Di Giovanni, D. Dobur, A. Drozdetskiy, R.D. Field, M. Fisher, Y. Fu, I.K. Furic, J. Gartner, S. Goldberg, J. Hugon, B. Kim, J. Konigsberg, A. Korytov, A. Kropivnitskaya, T. Kypreos, J.F. Low, K. Matchev, G. Mitselmakher, L. Muniz, P. Myeonghun, C. Prescott, R. Remington, A. Rinkevicius, M. Schmitt, B. Scurlock, P. Sellers, N. Skhirtladze, M. Snowball, D. Wang, J. Yelton, M. Zakaria

Florida International University, Miami, USA
V. Gaultney, L.M. Lebolo, S. Linn, P. Markowitz, G. Martinez, J.L. Rodriguez

Florida State University, Tallahassee, USA
T. Adams, A. Askew, J. Bochenek, J. Chen, B. Diamond, S.V. Gleyzer, J. Haas, S. Hagopian, V. Hagopian, M. Jenkins, K.F. Johnson, H. Prosper, S. Sekmen, V. Veeraraghavan

Florida Institute of Technology, Melbourne, USA
M.M. Baarmand, B. Dorney, M. Hohlmann, H. Kalakhety, I. Vodopiyanov

University of Illinois at Chicago (UIC), Chicago, USA
M.R. Adams, I.M. Anghel, L. Apanasevich, Y. Bai, V.E. Bazterra, R.R. Betts, J. Callner, R. Cavanaugh, C. Dragoiu, L. Gauthier, C.E. Gerber, D.J. Hofman, S. Khalatyan, G.J. Kunde[48], F. Lacroix, M. Malek, C. O'Brien, C. Silkworth, C. Silvestre, A. Smoron, D. Strom, N. Varelas

The University of Iowa, Iowa City, USA
U. Akgun, E.A. Albayrak, B. Bilki, W. Clarida, F. Duru, C.K. Lae, E. McCliment, J.-P. Merlo, H. Mermerkaya[49], A. Mestvirishvili, A. Moeller, J. Nachtman, C.R. Newsom, E. Norbeck, J. Olson, Y. Onel, F. Ozok, S. Sen, J. Wetzel, T. Yetkin, K. Yi

Johns Hopkins University, Baltimore, USA
B.A. Barnett, B. Blumenfeld, A. Bonato, C. Eskew, D. Fehling, G. Giurgiu, A.V. Gritsan, Z.J. Guo, G. Hu, P. Maksimovic, S. Rappoccio, M. Swartz, N.V. Tran, A. Whitbeck

The University of Kansas, Lawrence, USA
P. Baringer, A. Bean, G. Benelli, O. Grachov, R.P. Kenny Iii, M. Murray, D. Noonan, S. Sanders, R. Stringer, J.S. Wood, V. Zhukova

Kansas State University, Manhattan, USA
A.f. Barfuss, T. Bolton, I. Chakaberia, A. Ivanov, S. Khalil, M. Makouski, Y. Maravin, S. Shrestha,
I. Svintradze

Lawrence Livermore National Laboratory, Livermore, USA
J. Gronberg, D. Lange, D. Wright

University of Maryland, College Park, USA
A. Baden, M. Boutemeur, S.C. Eno, D. Ferencek, J.A. Gomez, N.J. Hadley, R.G. Kellogg, M. Kirn,
Y. Lu, A.C. Mignerey, K. Rossato, P. Rumerio, F. Santanastasio, A. Skuja, J. Temple, M.B. Tonjes,
S.C. Tonwar, E. Twedt

Massachusetts Institute of Technology, Cambridge, USA
B. Alver, G. Bauer, J. Bendavid, W. Busza, E. Butz, I.A. Cali, M. Chan, V. Dutta, P. Everaerts,
G. Gomez Ceballos, M. Goncharov, K.A. Hahn, P. Harris, Y. Kim, M. Klute, Y.-J. Lee,
W. Li, C. Loizides, P.D. Luckey, T. Ma, S. Nahn, C. Paus, D. Ralph, C. Roland, G. Roland,
M. Rudolph, G.S.F. Stephans, F. Stöckli, K. Sumorok, K. Sung, D. Velicanu, E.A. Wenger, R. Wolf,
B. Wyslouch, S. Xie, M. Yang, Y. Yilmaz, A.S. Yoon, M. Zanetti

University of Minnesota, Minneapolis, USA
S.I. Cooper, P. Cushman, B. Dahmes, A. De Benedetti, G. Franzoni, A. Gude, J. Haupt,
K. Klapoetke, Y. Kubota, J. Mans, N. Pastika, V. Rekovic, R. Rusack, M. Sasseville, A. Singovsky,
N. Tambe, J. Turkewitz

University of Mississippi, University, USA
L.M. Cremaldi, R. Godang, R. Kroeger, L. Perera, R. Rahmat, D.A. Sanders, D. Summers

University of Nebraska-Lincoln, Lincoln, USA
K. Bloom, S. Bose, J. Butt, D.R. Claes, A. Dominguez, M. Eads, P. Jindal, J. Keller, T. Kelly,
I. Kravchenko, J. Lazo-Flores, H. Malbouisson, S. Malik, G.R. Snow

State University of New York at Buffalo, Buffalo, USA
U. Baur, A. Godshalk, I. Iashvili, S. Jain, A. Kharchilava, A. Kumar, K. Smith, Z. Wan

Northeastern University, Boston, USA
G. Alverson, E. Barberis, D. Baumgartel, O. Boeriu, M. Chasco, S. Reucroft, J. Swain, D. Trocino,
D. Wood, J. Zhang

Northwestern University, Evanston, USA
A. Anastassov, A. Kubik, N. Mucia, N. Odell, R.A. Ofierzynski, B. Pollack, A. Pozdnyakov,
M. Schmitt, S. Stoynev, M. Velasco, S. Won

University of Notre Dame, Notre Dame, USA
L. Antonelli, D. Berry, A. Brinkerhoff, M. Hildreth, C. Jessop, D.J. Karmgard, J. Kolb, T. Kolberg,
K. Lannon, W. Luo, S. Lynch, N. Marinelli, D.M. Morse, T. Pearson, R. Ruchti, J. Slaunwhite,
N. Valls, M. Wayne, J. Ziegler

The Ohio State University, Columbus, USA
B. Bylsma, L.S. Durkin, C. Hill, P. Killewald, K. Kotov, T.Y. Ling, M. Rodenburg, C. Vuosalo,
G. Williams

Princeton University, Princeton, USA
N. Adam, E. Berry, P. Elmer, D. Gerbaudo, V. Halyo, P. Hebda, A. Hunt, E. Laird, D. Lopes
Pegna, D. Marlow, T. Medvedeva, M. Mooney, J. Olsen, P. Piroué, X. Quan, B. Safdi, H. Saka,
D. Stickland, C. Tully, J.S. Werner, A. Zuranski

University of Puerto Rico, Mayaguez, USA
J.G. Acosta, X.T. Huang, A. Lopez, H. Mendez, S. Oliveros, J.E. Ramirez Vargas, A. Zatserklyaniy

Purdue University, West Lafayette, USA
E. Alagoz, V.E. Barnes, G. Bolla, L. Borrello, D. Bortoletto, M. De Mattia, A. Everett, A.F. Garfinkel, L. Gutay, Z. Hu, M. Jones, O. Koybasi, M. Kress, A.T. Laasanen, N. Leonardo, C. Liu, V. Maroussov, P. Merkel, D.H. Miller, N. Neumeister, I. Shipsey, D. Silvers, A. Svyatkovskiy, M. Vidal Marono, H.D. Yoo, J. Zablocki, Y. Zheng

Purdue University Calumet, Hammond, USA
S. Guragain, N. Parashar

Rice University, Houston, USA
A. Adair, C. Boulahouache, K.M. Ecklund, F.J.M. Geurts, B.P. Padley, R. Redjimi, J. Roberts, J. Zabel

University of Rochester, Rochester, USA
B. Betchart, A. Bodek, Y.S. Chung, R. Covarelli, P. de Barbaro, R. Demina, Y. Eshaq, H. Flacher, A. Garcia-Bellido, P. Goldenzweig, Y. Gotra, J. Han, A. Harel, D.C. Miner, G. Petrillo, W. Sakumoto, D. Vishnevskiy, M. Zielinski

The Rockefeller University, New York, USA
A. Bhatti, R. Ciesielski, L. Demortier, K. Goulianos, G. Lungu, S. Malik, C. Mesropian

Rutgers, the State University of New Jersey, Piscataway, USA
S. Arora, O. Atramentov, A. Barker, C. Contreras-Campana, E. Contreras-Campana, D. Duggan, Y. Gershtein, R. Gray, E. Halkiadakis, D. Hidas, D. Hits, A. Lath, S. Panwalkar, R. Patel, A. Richards, K. Rose, S. Schnetzer, S. Somalwar, R. Stone, S. Thomas

University of Tennessee, Knoxville, USA
G. Cerizza, M. Hollingsworth, S. Spanier, Z.C. Yang, A. York

Texas A&M University, College Station, USA
R. Eusebi, W. Flanagan, J. Gilmore, A. Gurrola, T. Kamon, V. Khotilovich, R. Montalvo, I. Osipenkov, Y. Pakhotin, A. Perloff, A. Safonov, S. Sengupta, I. Suarez, A. Tatarinov, D. Toback

Texas Tech University, Lubbock, USA
N. Akchurin, C. Bardak, J. Damgov, P.R. Dudero, C. Jeong, K. Kovitanggoon, S.W. Lee, T. Libeiro, P. Mane, Y. Roh, A. Sill, I. Volobouev, R. Wigmans, E. Yazgan

Vanderbilt University, Nashville, USA
E. Appelt, E. Brownson, D. Engh, C. Florez, W. Gabella, M. Issah, W. Johns, C. Johnston, P. Kurt, C. Maguire, A. Melo, P. Sheldon, B. Snook, S. Tuo, J. Velkovska

University of Virginia, Charlottesville, USA
M.W. Arenton, M. Balazs, S. Boutle, B. Cox, B. Francis, S. Goadhouse, J. Goodell, R. Hirosky, A. Ledovskoy, C. Lin, C. Neu, J. Wood, R. Yohay

Wayne State University, Detroit, USA
S. Gollapinni, R. Harr, P.E. Karchin, C. Kottachchi Kankanamge Don, P. Lamichhane, M. Mattson, C. Milstène, A. Sakharov

University of Wisconsin, Madison, USA
M. Anderson, M. Bachtis, D. Belknap, J.N. Bellinger, D. Carlsmith, M. Cepeda, S. Dasu, J. Efron, E. Friis, L. Gray, K.S. Grogg, M. Grothe, R. Hall-Wilton, M. Herndon, A. Hervé, P. Klabbers,

J. Klukas, A. Lanaro, C. Lazaridis, J. Leonard, R. Loveless, A. Mohapatra, I. Ojalvo, W. Parker, I. Ross, A. Savin, W.H. Smith, J. Swanson, M. Weinberg

†: Deceased
1: Also at CERN, European Organization for Nuclear Research, Geneva, Switzerland
2: Also at Universidade Federal do ABC, Santo Andre, Brazil
3: Also at California Institute of Technology, Pasadena, USA
4: Also at Laboratoire Leprince-Ringuet, Ecole Polytechnique, IN2P3-CNRS, Palaiseau, France
5: Also at Suez Canal University, Suez, Egypt
6: Also at British University, Cairo, Egypt
7: Also at Fayoum University, El-Fayoum, Egypt
8: Also at Ain Shams University, Cairo, Egypt
9: Also at Soltan Institute for Nuclear Studies, Warsaw, Poland
10: Also at Université de Haute-Alsace, Mulhouse, France
11: Also at Moscow State University, Moscow, Russia
12: Also at Brandenburg University of Technology, Cottbus, Germany
13: Also at Institute of Nuclear Research ATOMKI, Debrecen, Hungary
14: Also at Eötvös Loránd University, Budapest, Hungary
15: Also at Tata Institute of Fundamental Research - HECR, Mumbai, India
16: Also at University of Visva-Bharati, Santiniketan, India
17: Also at Sharif University of Technology, Tehran, Iran
18: Also at Isfahan University of Technology, Isfahan, Iran
19: Also at Shiraz University, Shiraz, Iran
20: Also at Facoltà Ingegneria Università di Roma, Roma, Italy
21: Also at Università della Basilicata, Potenza, Italy
22: Also at Laboratori Nazionali di Legnaro dell' INFN, Legnaro, Italy
23: Also at Università degli studi di Siena, Siena, Italy
24: Also at Faculty of Physics of University of Belgrade, Belgrade, Serbia
25: Also at University of California, Los Angeles, Los Angeles, USA
26: Also at University of Florida, Gainesville, USA
27: Also at Université de Genève, Geneva, Switzerland
28: Also at Scuola Normale e Sezione dell' INFN, Pisa, Italy
29: Also at INFN Sezione di Roma; Università di Roma "La Sapienza", Roma, Italy
30: Also at University of Athens, Athens, Greece
31: Also at The University of Kansas, Lawrence, USA
32: Also at Paul Scherrer Institut, Villigen, Switzerland
33: Also at University of Belgrade, Faculty of Physics and Vinca Institute of Nuclear Sciences, Belgrade, Serbia
34: Also at Institute for Theoretical and Experimental Physics, Moscow, Russia
35: Also at Gaziosmanpasa University, Tokat, Turkey
36: Also at Adiyaman University, Adiyaman, Turkey
37: Also at The University of Iowa, Iowa City, USA
38: Also at Mersin University, Mersin, Turkey
39: Also at Izmir Institute of Technology, Izmir, Turkey
40: Also at Kafkas University, Kars, Turkey
41: Also at Suleyman Demirel University, Isparta, Turkey
42: Also at Ege University, Izmir, Turkey
43: Also at Rutherford Appleton Laboratory, Didcot, United Kingdom
44: Also at School of Physics and Astronomy, University of Southampton, Southampton, United Kingdom

45: Also at INFN Sezione di Perugia; Università di Perugia, Perugia, Italy
46: Also at Utah Valley University, Orem, USA
47: Also at Institute for Nuclear Research, Moscow, Russia
48: Also at Los Alamos National Laboratory, Los Alamos, USA
49: Also at Erzincan University, Erzincan, Turkey